


## Topical Review

# All-solid-state thin-film batteries based on lithium phosphorus oxynitrides

Wangqi Dai<sup>1</sup>, Yan Qiao<sup>1</sup>, Ziqiang Ma<sup>2</sup>, Tian Wang<sup>1</sup> and Zhengwen Fu<sup>1,\*</sup> <sup>1</sup> Shanghai Key Laboratory of Molecular Catalysis and Innovative Materials, Department of Chemistry, Fudan University, Shanghai 200433, People's Republic of China<sup>2</sup> Nano Science and Technology Institute, University of Science and Technology of China, Suzhou 215123, People's Republic of ChinaE-mail: [zwfu@fudan.edu.cn](mailto:zwfu@fudan.edu.cn)

Received 18 May 2022, revised 27 June 2022

Accepted for publication 1 July 2022

Published 23 September 2022



## Abstract

Lithium phosphorus oxygen nitrogen (LiPON) as solid electrolyte discovered by Bates *et al* in the 1990s is an important part of all-solid-state thin-film battery (ASSTFB) due to its wide electrochemical stability window and negligible low electronic conductivity. However, the ionic conductivity of LiPON about  $2 \times 10^{-6} \text{ S cm}^{-1}$  at room temperature is much lower than that of other types of solid electrolytes, which seriously limits the application of ASSTFBs. This review summarizes the research and progress in ASSTFBs based on LiPON, in the solid-state electrolyte of LiPON-derivatives with adjustable chemical compositions of the amorphous structure for the improvement of the ionic conductivity and electrochemical stability, in the critical interface issues between LiPON and electrodes, and in preparation methods for LiPON. This review is helpful for people to understand the interface characteristics and various preparation methods of LiPON in ASSTFBs. The key issues to be addressed concern how to develop solid-state electrolyte films with high conductivity and high-quality interface engineering as well as large-scale preparation technology, so as to realize the practical application of highly integrated ASSTFBs.

**Keywords:** LiPON, solid electrolyte, solid thin-film battery, interfacial property, preparation method

## 1. The development of LiPON in ASSTFB

An all-solid-state thin-film battery (ASSTFB) is a kind of solid-state battery in the form of a thin film whose total thickness is at the micron level, which has high capacity, long cycle

life, excellent mechanical strength, and good thermotolerance. These advantages make it suitable for potential applications such as smart cards, microsenors, microelectronics, and micromechanical devices as micropower sources that could not be replaced by other chemical batteries [1–3]. It is composed of thin films of the cathode, solid electrolyte and anode constructed on a substrate in sequence, and the schematic of the representative fabrication process for ASSTFB based on lithium phosphorus oxygen nitrogen (LiPON) thin-film solid electrolyte is shown in figure 1. Since the 1980s, a lot of research on thin-film electrode materials and solid-state electrolytes in thin-film batteries has been conducted, and has obtained many satisfactory results (figure 2). There are two

\* Author to whom any correspondence should be addressed.



Original content from this work may be used under the terms of the [Creative Commons Attribution 4.0 licence](https://creativecommons.org/licenses/by/4.0/). Any further distribution of this work must maintain attribution to the author(s) and the title of the work, journal citation and DOI.

### Future perspectives

Driven by the demand for future miniaturized low-power devices, great efforts are being directed towards increasing the energy density of ASSTFBs based on LiPON. Their potential advantageously offers energy miniaturization and integration such as three dimensions (3D) high-density integration of micro-batteries and an energy integrated system with micro-photovoltaic cells, micro-piezoelectric energy collectors, and so on. The development of ASSTFBs should focus on the design of thin-film batteries based on intelligent and 3D technology, the large-scale preparation technology suitable for high-performance LiPON derivative films, and the perfect interface engineering between them and electrodes.

kinds of thin-film lithium batteries that have attracted much attention for a long time. One is the thin-film battery assembled with the polymer solid electrolyte, and the other is the thin-film battery assembled with the inorganic solid electrolyte. However, the thin-film battery with polymer electrolyte has a narrow working temperature range, poor integration compatibility, and a lack of adaptability to various extreme environments, which is quite different from that with inorganic thin-film electrolyte. ASSTFB is constructed primarily by the physical vapor deposition technique, which can be coupled with modern semiconductor processes. Therefore, this kind of ASSTFB with a thickness of fewer than 10  $\mu\text{m}$  is expected to be integrated into semiconductor devices to realize the miniaturization and integration of thin-film batteries.

Hitachi firstly reported on thin-film batteries in 1982 [4], but it could not drive the electronic devices at that time due to the low power of the thin-film batteries. In the past two decades, advances in semiconductor technology have led to many kinds of low-power devices such as complementary metal-oxide-semiconductor [5], ferroelectric random access memory [6] and liquid crystal displays [7], and it is feasible to make thin-film batteries work as power sources for these miniaturized low-power devices. With the rapid development of micro-electronic devices, the demand for the higher energy density of thin-film batteries is increasing in recent years. Fortunately, many commercial companies with ASSTFB are promoting the practical application of thin-film batteries. For example, Infinite Power Solutions has launched the active radio frequency identification devices (RFID) composed of an ASSTFB, an integrated chip, and a thin-film antenna. It can receive radio frequency (RF) through the antenna to charge ASSTFB, which provides the power source for active RFID tags. Cymbet provides ASSTFB for microelectronic devices as backup power. The thin-film battery integrates two parts of energy storage and power management and is packaged into a patch-type thin-film battery. The operation voltage of the battery is 3.9 V with the capacity of 100  $\mu\text{Ah}$ , and the attenuation of the capacity is less than 10% after 5000 cycles, with the operating temperature ranging from  $-20$  to  $70$   $^{\circ}\text{C}$ . In addition, ASSTFB with flexibility and no cytotoxicity is a key component of an integrated intra-oral light therapy device that is installed in the humans dental arch in an adaptive manner (figure 3) [8].

The concept of ASSTFBs was first proposed in the 1980s [4].  $\text{TiS}_2$  prepared by chemical vapor deposition (CVD) method was used as cathode material in this

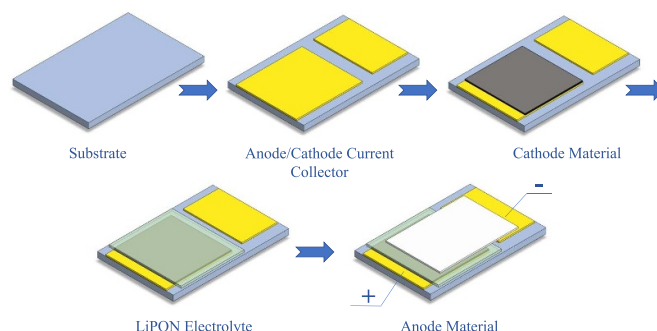


**Figure 1.** Schematic of the fabrication process for all-solid-state lithium batteries based on LiPON thin-film solid electrolyte.

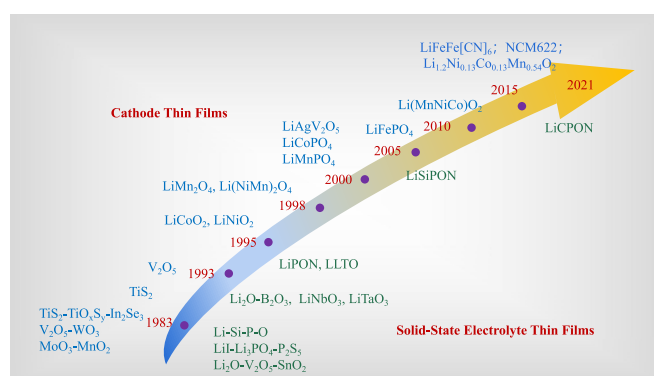


**Figure 2.** The schematic illustration of the development of cathode thin films and solid-state electrolyte thin films in ASSTFBs.

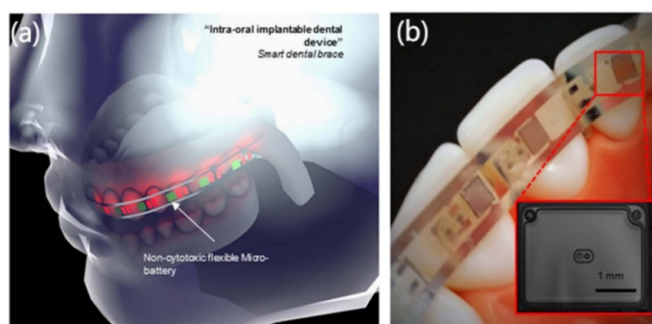


**Figure 3.** (a) Non-cytotoxic flexible batteries are integrated into intra-oral phototherapeutic devices. (b) Optica images of the micro lithium battery in the intra-oral device. Reproduced from [8]. CC BY 4.0.

battery,  $\text{Li}_{3.6}\text{Si}_{0.6}\text{P}_{0.4}\text{O}_4$  solid electrolyte and metal Li anode were fabricated by RF sputtering method and vacuum thermal evaporation, respectively [9]. In addition,  $\text{WO}_3$  and  $0.63\text{WO}_3-0.37\text{V}_2\text{O}_5$  cathodes that had been synthesized by reactive sputtering in the  $\text{H}_2$ -Ar atmosphere were also integrated into this kind of battery [10]. The first thin-film battery has a size of  $4\text{ mm} \times 4\text{ mm}$ , and an overall thickness of  $6-8\text{ }\mu\text{m}$ , including  $1-3.7\text{ }\mu\text{m}$  of  $\text{TiS}_2$  cathode,  $2-4\text{ }\mu\text{m}$  of electrolyte, and  $4\text{ }\mu\text{m}$  of Li metal anode. The reaction platform of these batteries is at 2.5 V, the current density and the capacity of which are  $3-16\text{ }\mu\text{A cm}^{-2}$  and  $45-150\text{ }\mu\text{Ah cm}^{-2}$

separately. Nippon Telegraph & Telephone also developed a series of thin-film batteries fabricated by the RF sputtering method, in which the  $\text{Li}_3\text{VO}_4\text{--Li}_4\text{SiO}_4$  solid solution system ( $\text{Li}_{3.4}\text{V}_{0.6}\text{Si}_{0.4}\text{O}_4$  and  $\text{Li}_2\text{O--V}_2\text{O}_5\text{--SiO}_2$ ) were employed as the solid electrolyte, transition metal oxide ( $\text{MnO}_2$ ,  $\text{WO}_3$ , and  $\text{MoO}_3$ ) and evaporated Li metal was used as the cathode and anode, respectively [11–13]. These kinds of batteries are  $1\text{ cm}^2$  in size, with a cathode thickness of  $1\text{--}5\text{ }\mu\text{m}$ , an electrolyte thickness of  $1\text{ }\mu\text{m}$ , and a Li metal anode thickness of  $4\text{--}8\text{ }\mu\text{m}$ . In the 1980s, Eveready Battery Company and Bellcore in the United States prepared thin-film batteries containing sulfide glass electrolytes such as  $\text{Li}_4\text{P}_2\text{S}_7$  or  $\text{Li}_3\text{PO}_4\text{--P}_2\text{S}_5$ , using  $\text{TiS}_2$  as cathode material and Li metal or LiI as anode [14–16], whose voltage range is  $1.5\text{--}2.8\text{ V}$ , the current density is  $10\text{--}135\text{ }\mu\text{Ah cm}^{-2}$  and the cycle retention can reach more than 1000 times. Besides, Bellcore fabricated kinds of thin-film batteries with  $\text{LiMn}_2\text{O}_4$  as the cathode material, lithium borophosphate glass as the solid electrolyte and Li metal as the anode, which can cycle more than 150 times between  $3.5$  and  $4.3\text{ V}$  with 75% capacity retention after cycling [17].

A landmark move is that Oak Ridge National Laboratory (ORNL) used LiPON solid electrolyte for preparing thin-film batteries in the 1990s [18–20]. LiPON thin-film solid electrolyte was prepared by RF sputtering a  $\text{Li}_3\text{PO}_4$  target in the  $\text{N}_2$  atmosphere, which is very stable compared with other lithium oxide and sulfide glass electrolytes and possesses moderate ionic conductivity (about  $2.3 \times 10^{-6}\text{ S cm}^{-1}$ ) and activated energy ( $0.55\text{ eV}$ ) [20]. The I–V curve of LiPON showed that it has a wide electrochemical stability window whose range is  $0\text{--}5.5\text{ V}$  (vs.  $\text{Li/Li}^+$ ). They reported some thin-film batteries with LiPON solid electrolyte demonstrating excellent electrochemical performance, whose voltage range is from  $2\text{ V}$  to  $5\text{ V}$ , and the current density can reach  $10\text{ mA cm}^{-2}$  and the cycle can exceed 10 000 times. It is worth noting that Newdecker *et al* reported a ‘lithium-free’ thin-film battery, that is, after the film battery with  $\text{LiCoO}_2$  (LCO) as the cathode was charged for the first time, a layer of Li metal anode was *in situ* plated on the Cu current collector. This kind of method to prepare thin-film batteries avoids the presence of low melting lithium under the condition of welding reflow, which makes it possible to integrate the thin-film batteries into electronic circuits [21]. LiPON is now considered as one of the normative solid electrolytes for thin-film lithium batteries and is used by many research teams and several companies in the United States, such as Jet Propulsion Laboratory [22, 23], Korea Institute of Science and Technology [24, 25], Cymbet, Excellatron, etc. Baba and co-workers reported a new type of thin-film battery with LiPON as the solid electrolyte.  $\text{Li}_x\text{V}_2\text{O}_5$  or  $\text{V}_2\text{O}_5$  was used as anode instead of metal lithium to construct  $\text{V}_2\text{O}_5/\text{LiPON}/\text{Li}_x\text{V}_2\text{O}_5$  and  $\text{V}_2\text{O}_5/\text{LiPON}/\text{LiMn}_2\text{O}_4$  thin-film batteries. Since the metal Li is not used as the anode, this kind of rocking chair battery has obvious advantages in the preparation process and the safety, but it needs to be charged before the first use [26, 27]. This kind of battery experiences a dramatic increase in capacity to  $10\text{ }\mu\text{Ah cm}^{-2}$  at the first 20 times

cycle, which can be attributed to the gradual reduction of interfacial resistance between the electrode and solid electrolyte [27]. Baba *et al* also prepared multiple cells on a single substrate to increase the voltage and current density of batteries, which can reach  $3\text{--}6.5\text{ V}$  and  $2\text{ }\mu\text{A cm}^{-2}$ , respectively [28]. West *et al* fabricated ASSTFB by using high-voltage cathode materials of  $\text{Li}_y\text{Mn}_{1.4}\text{Ni}_{0.6}\text{O}_4$  and  $\text{LiCoPO}_4$  as cathode, whose discharge plateau can reach more than  $4.5\text{ V}$  [22, 23].

Thin-film batteries have also been studied by Ribes’s group in France since the 1980s, they focused on chalcogens compounds as cathode materials, such as  $\text{In}_2\text{Se}_3$ ,  $\text{TeO}_2$ ,  $\text{GeSe}_{5.5}$ ,  $\text{TiS}_2$ , etc [29–33]. Balkanski *et al* investigated the electrochemical properties of the thin-film batteries consisting of  $\text{In}_2\text{Se}_3$  or  $\text{InSe}$  cathode, Li metal anode and lithium borate glass electrolyte, in which the cathode and electrolyte materials were prepared by flash evaporation and molecular beam deposition techniques, respectively [31]. Creus *et al* prepared  $\text{Li}/\text{Li}_2\text{S--SiS}_2/\text{GeSe}_{5.5}$  and  $\text{Li}/0.7(0.4\text{Li}_2\text{O--}0.2\text{B}_2\text{O}_3\text{--}0.4\text{P}_2\text{O}_5)\text{--}0.3\text{LiCl}/0.7\text{V}_2\text{O}_5\text{--}0.3\text{TeO}_2$  thin film batteries by RF sputtering and flash evaporation. Menetrier *et al* developed a thin-film battery using  $\text{TiS}_2$  as cathode material and  $\text{B}_2\text{S}_3\text{--Li}_2\text{S--LiI}$  as the vitreous electrolyte, whose open-circuit voltage is about  $2.0\text{ V}$  and the capacity is  $50\text{--}300\text{ }\mu\text{Ah cm}^{-2}$  [30]. Kuwata *et al* prepared a thin-film battery with LCO as the cathode,  $\text{Li}_{6.1}\text{V}_{0.61}\text{Si}_{0.39}\text{O}_{5.36}$  glass as the solid electrolyte, and  $\text{SnO}$  as the anode material [34]. Each thin-film component in this kind of battery was *in situ* fabricated by only using the pulsed laser deposition (PLD) technique. The size of the battery is about  $0.23\text{ cm}^2$  and the thickness is about  $2\text{ }\mu\text{m}$ . However, after the first charge, the  $\text{SnO}$  anode reacts with the lithium-ion to generate  $\text{Sn--Li}$  alloy and amorphous  $\text{Li}_2\text{O}$ , resulting in a large capacity loss. Such a thin-film cell was prepared by using micromachining technology, and its cross-section image was primarily observed by scanning electron microscope (SEM). The recent literatures on micromachined thin-film batteries were reviewed and they will not be introduced here [2, 35].

Although rechargeable lithium-ion batteries are strong candidates for high-performance flexible power sources, the compatible electrode material for bendable lithium-ion batteries is limited, and the electrochemical performance of the flexible battery is insufficient for application in flexible consumer electronic devices such as the flexible display. In 2012, Koo *et al* proposed the universal transfer approach to develop a bendable thin-film battery regardless of the chemical properties of the electrodes (figure 4(a)) [36]. This approach could transfer high-temperature annealed electrodes to the polymer substrates for the high-performance thin-film battery. Such a bendable lithium-ion battery can be integrated with a flexible light-emitting diode (LED) to construct an all-in-one flexible electronic device (figure 4(b)). Hallot *et al* prepared a thicker  $\text{LiMn}_{1.5}\text{Ni}_{0.5}\text{O}_4$  (LNMO) layer for lithium-ion batteries by using the stacking layers of Cr and Pt metal as the current collector on aluminum oxide@Si wafer due to the adhesion improvement between aluminum oxide and platinum layers. When the thickness of LNMO film increases from



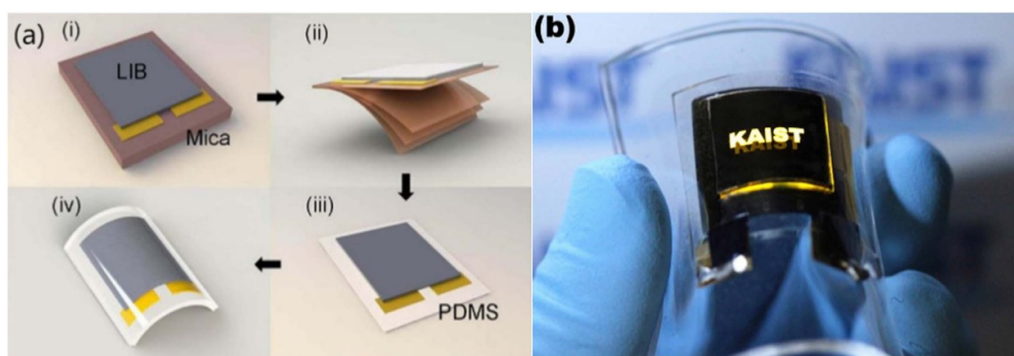


**Figure 4.** (a) Schematic illustration of the process for the fabrication of flexible lithium-ion batteries, and the key operation is to use sticky tapes to delaminate the battery from the mica substrate ((i) and (ii)). (b) The picture of a flexible LED system with a bendable lithium-ion battery as the power source. Reprinted with permission from [36]. Copyright (2012), American Chemical Society.

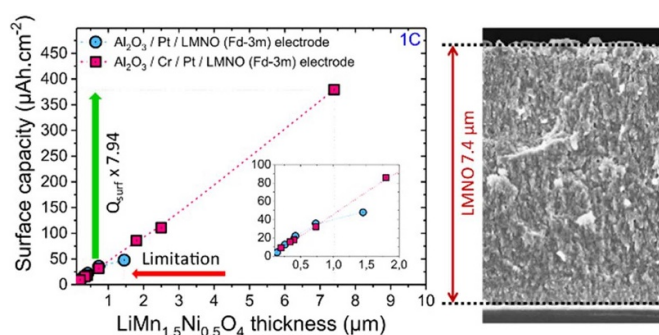


**Figure 5.** Evolution of the surface capacity regarding the film thickness and the type of current collector (Pt or Cr/Pt) and SEM cross-section analysis of the 7.4  $\mu\text{m}$ -thick LNMO film. Reprinted from [37]. Copyright (2018), with permission from Elsevier.

150 nm to 7400 nm, the areal capacity of which is significantly enhanced from 3 to 375  $\mu\text{Ah cm}^{-2}$ , and new opportunities seem to be opened for preparing thin-film batteries with high energy density and ultra-high rate capability (figure 5) [37]. Trask *et al* illustrated the electrochemical properties of LCO textures [38]. The (003) plane (an unfavorable texture) is a strong texture of LCO due to its lowest surface energy, and the crystallization during anneal leads to the formation of more favorable LCO textures such as (101), (104), and (110) orientation (figure 6). The thin-film battery with texture-controlled cathode exhibited a discharge capacity of 600  $\text{mAh cm}^{-2}$  at C/10 rate, and larger than 95% capacity retention after 100 times cycle at C/5 rate. The thin-film battery with the uncontrolled cathode (predominantly (003)) has a similar capacity, but the cycling performance and rate capability of which are severely diminished.

Up to now, ASSTFBs based on the LiPON thin-film solid electrolyte have been fabricated by various preparation methods. Yamamoto *et al* prepared one layer of LCO cathode on LiPON film by using the aerosol deposition method without heating to construct an inverted-stack Li-free thin-film battery, which can stably cycle for over 100 times [39]. Tunnel structure  $\text{Li}_x\text{MnO}_2$  nanosheet arrays cathode material was prepared by an essential interfacial reaction between  $\text{MnO}_{2-x}$  with LiPON for infusing  $\text{Li}^+$  ion into  $\text{MnO}_{2-x}$  at a low

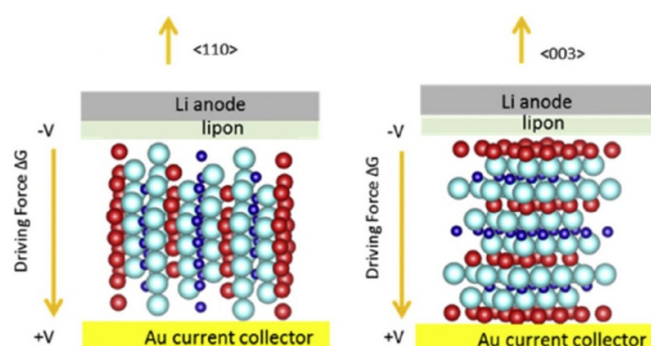


**Figure 6.** Illustration of the orthorhombic phase of  $\text{Li}_x\text{CoO}_2$ . The left image shows a favorable texture of LCO for the migration of lithium ions because the driving force is parallel to the intercalation planes, and the texture of LCO in the right one is unfavorable. Light blue spheres are O, red spheres are Li, and dark blue spheres are Co. Reprinted from [38]. Copyright (2017), with permission from Elsevier.

temperature of 180  $^{\circ}\text{C}$ , and the ASSTFB  $\text{Li}_x\text{MnO}_2/\text{LiPON}/\text{Li}$  shows better rate and cycling properties than 2D  $\text{MnO}_{2-x}$  or traditional  $\text{LiMn}_2\text{O}_4$  (LMO) thin-film batteries [40]. Vertically aligned oxygen-deficient  $\alpha\text{-MoO}_{3-x}$  nanoflake arrays were reported as cathode material for thin-film batteries with LiPON as the electrolyte, which shows better performance than the 2D cathode owing to the larger electrode/electrolyte interface area and shorter  $\text{Li}^+$  ion diffusion pathway [41]. Chen *et al* investigated the photonic methods for fast crystallization of LMO cathode in LiPON-based thin-film batteries, among which the xenon flash-lamp annealing is a promising technique for preparing high electrochemical performance electrode [42]. They also used the same method to prepare LCO cathode on Al foil to fabricate flexible thin-film batteries [43]. The *in situ* annealing LCO cathode on a 500  $^{\circ}\text{C}$  substrate during the deposition process exhibits better crystal structure and electrochemical performance than the post-annealing one in thin-film batteries reported by Wang *et al*, which illustrated the value of *in situ* annealing [44]. Zhang *et al* used the RF magnetron sputtering method to prepare thin-film batteries with lithium trivanadate (LVO) cathode and LiPON electrolyte [45]. They found that the partially crystalline LVO

performed better than the amorphous or the totally crystalline one, and the rate-limited steps such as phase-transformation reactions and ionic diffusion process during cycling of batteries are associated with the level of crystallization and operated temperature. Yim *et al* prepared thin-film LNMO cathode material on polyimide substrate by excimer laser annealing process, which is a promising technique with minute damage for polymer substrate, and the full cells are bendable and have stable cycling performance [46]. The thin-film batteries with  $\text{Li}_4\text{Ti}_5\text{O}_{12}$  (LTO) cathode prepared by using flame spray pyrolysis technique on polymer substrate also demonstrated great rate capability and stable cycling with negligible damage of substrate [47].

Except for LiPON solid thin-film electrolytes, other kinds of thin-film electrolytes used in ASSTFBs also have been reported in recent years. Nishio *et al* fabricated a bottom-current-collector-free thin-film battery with the high ordered and crystalline  $\text{LiNi}_{0.8}\text{Co}_{0.2}\text{O}_2$  epitaxial thin film as cathode material and  $\text{Li}_3\text{PO}_4$  as the solid electrolyte, which shows stable battery operation due to anti-phase grain boundaries migration although the orientation of cathode thin film is unfavorable for ionic transport [48]. They also studied the structural and electrochemical properties of NMC(001) epitaxial thin film on the same electrolyte, which manifests low interfacial resistance and stable cycling [49].

Our research group has also carried out relevant research since 2000 and has made great progress. Many kinds of metallic oxide, nitride, and fluoride electrode film have been prepared effectively by PLD or RF magnetron sputtering such as  $\text{LiMn}_2\text{O}_4$ , LCO,  $\text{Ta}_2\text{O}_5$ ,  $\text{TiO}_2$ , ZnO, NiO,  $\text{Ag}_{0.5}\text{V}_2\text{O}_5$ ,  $\text{MN}_x$  ( $\text{M} = \text{Co, Fe, Ni, Mn}$ ), etc [50–57], all of which have good electrical or electrochemical properties. Great improvement has been made in the preparation of thin-film electrolytes, such as LiPON and Li–V–Si–O thin film was successfully prepared by PLD or electron beam evaporation [58–60]; Li/LiPON/ $\text{V}_2\text{O}_5$ , Li/LiPON/LCO thin-film batteries were satisfactorily prepared by combining PLD with vacuum thermal evaporation for the first time [59, 61]. The ‘lithium-free’ and ‘anode-free’ ASSTFB of stainless steel (SS)/LiPON/Ag was first reported, in which the solid electrolyte worked as the lithium source [62]. Lithium-ion was reduced at the anode (SS) surface to form a metallic lithium layer when the voltage of the battery was higher than 3.7 V, and a new phase  $\text{Ag}_{x-1}\text{LiPO}_y\text{N}_z$  emerged at the cathode probably. At present, the ASSTFBs with a kind of Prussian blue compound ( $\text{LiFeFe}[\text{CN}]_6$ , PB) as the cathode material were fabricated, in which the PB cathode was prepared by coating technology (figure 7) [63]. The  $\text{LiFeFe}[\text{CN}]_6$ /LiPON/Li solid battery was made by the deposition of LiPON on PB cathode by RF magnetron sputtering and consequent thermal evaporation of Li metal, whose thickness and size were  $16\text{ }\mu\text{m}$  and  $10\text{ cm}^2$ , respectively. The electrochemical performance of the batteries at the temperature range of  $-30 \sim 80\text{ }^\circ\text{C}$  was studied for the first time, which indicated that the discharge capacity of the third cycle at  $60\text{ }^\circ\text{C}$  is  $82.5\text{ mAh cm}^{-2}$  and the battery can stably cycle 200 times. These results provide the feasibility of assembling ASSTFBs by combining coating technology with vacuum technology.

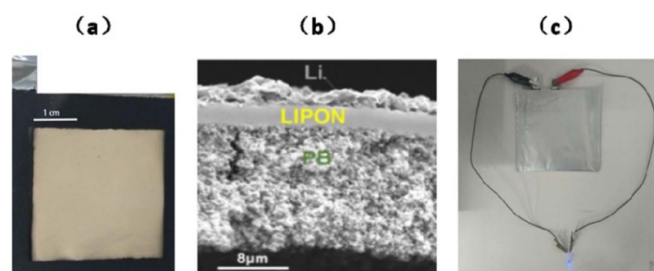


**Figure 7.** (a) Typical photo and (b) cross-sectional SEM image of all-solid-state  $\text{LiFeFe}[\text{CN}]_6$ /LiPON/Li battery; (c) film battery lighting a blue LED. Reprinted with permission from [63]. Copyright (2018) American Chemical Society.

## 2. LiPON based derivatives and analogs

After the fruitful preparation of LiPON by Bates *et al* at ORNL in the 1990s, this kind of thin-film glass electrolyte has been widely used to fabricate the thin-film batteries as mentioned above. It is generally accepted that the incorporation of N element in the amorphous  $\text{Li}_3\text{PO}_4$  electrolyte could significantly improve the ionic conductivity of LiPON [20]. The structure of LiPON has been investigated by spectroscopic characterization techniques such as x-ray photoelectron spectroscopy (XPS), infrared spectrum, Raman spectrum, and nuclear magnetic resonance (NMR). However, it is not clear for the key issues to reveal the bonding mode of N atoms in LiPON. Previously, Bates *et al* hypothesized that there were two kinds of N species in LiPON, which were double- ( $\text{N}_d$ ) and triple- ( $\text{N}_t$ ) coordinated N, respectively [64]. One evidence to support this hypothesis is that the N 1s XPS spectrum from LiPON shows two different kinds of N with the binding energy of 397.8 eV ( $\text{N}_d$ ) and 399.4 eV ( $\text{N}_t$ ), respectively. Recently, Lacivita *et al* put forward a different opinion according to the simulation of neutron pair distribution function (PDF) that N atoms in LiPON only form  $\text{N}_d$  and nonbridging apical N connecting to P atoms ( $\text{N}_a$ ) (figure 8) [65]. They also proposed that the binding energy of  $\text{N}_a$  is less than  $\text{N}_d$  and the signal at 399.4 eV corresponds to the  $\text{N}_d$  or the surface contamination of LiPON. With the increase of Li content, the amount of  $\text{N}_d$  is decreasing while the amount of  $\text{N}_a$  has an opposite trend, which is harmful to the ionic conductivity due to tighter bonding between  $\text{Li}^+$  ions with  $\text{N}_a$  than  $\text{N}_d$ . To further improve the ionic conductivity and electrochemical stabilities of LiPON electrolyte, LiPON-based derivatives were studied and their chemical and electrochemical properties were investigated.

To date, many different silicon-doped derivative electrolytes of LiPON with outstanding electrochemical performance have been well-prepared. Lee *et al* fabricated a silicon-doped LiPON-based solid electrolyte LiSiPON by sputtering  $\text{Li}_3\text{PO}_4$ - $\text{Li}_2\text{SiO}_3$  mixed target, which shows a higher ionic conductivity ( $1.24 \times 10^{-5}\text{ S cm}^{-1}$ ) in a certain Si:P ratio than most of the LiPON-type solid electrolyte (about  $10^{-6}\text{ S cm}^{-1}$ ) due to the ‘mixed former effect’. It is found out that the activation energy of  $\text{Li}^+$  ion conduction decreases with the increase of Si content, leading to an increase in the conductivity of

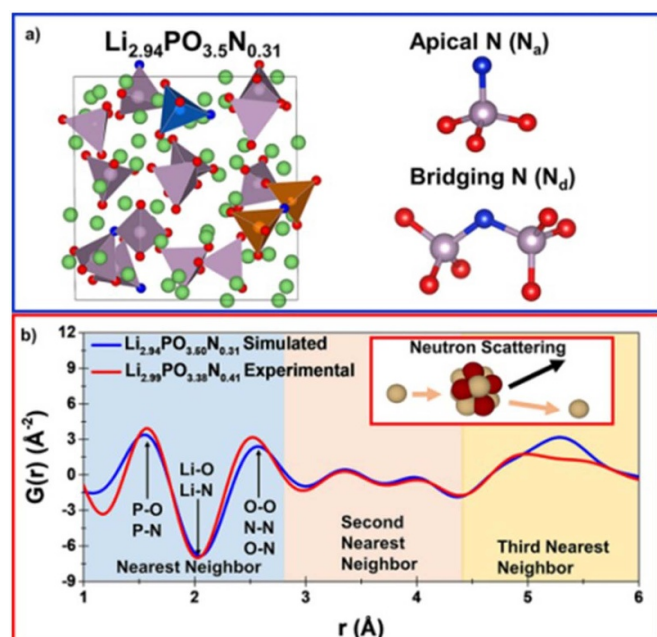


**Figure 8.** (a) Schematic of simulated  $\text{Li}_{2.94}\text{PO}_{3.50}\text{N}_{0.31}$  structure from AIMD. Red atoms are O, blue atoms are N, green atoms are Li, and light gray atoms are P. (b) Comparison of simulated and experimental neutron PDF data of LiPON. Reprinted with permission from [65]. Copyright (2018) American Chemical Society.

the film [66]. They also fabricated the thin-film batteries composed of LiSiPON electrolyte and the Si-V anode, which manifest stable cycling over 1500 times [67]. Su *et al* investigated the mechanism of ionic conduction in LiSiPON thin-film electrolyte and found that the introduction of Si in LiPON substituting the P atoms with the formation of cross-linked Si-O-P and (P, Si)-N < (P, Si) structures is beneficial for the migration of  $\text{Li}^+$  ion [68]. Famprakis *et al* studied the amorphization, mixed former effect, and nitridation effect on LiSiPO(N) electrolyte prepared by sputtering a single-phase crystalline target of  $\text{Li}_{3-x}\text{Si}_x\text{P}_{1-x}\text{O}_4$  ( $(1-x)\text{Li}_3\text{PO}_4-x\text{Li}_4\text{SiO}_4$ ), and reported that mixed former and nitridation should be responsible for the improvement of ionic conductivity of LiSiPO(N) [69]. They also proved the existence of a minimum critical value of Li content for efficient  $\text{Li}^+$  conduction. So far, composite electrolytes of LiSiPON-based inorganic polymer have been well fabricated, however, they were not prepared for thin-film batteries and thus no detailed introduction would be made [70–73]. Wu *et al* prepared an amorphous LiTiSiPON thin-film electrolyte by using the RF magnetron sputtering method, and they discovered that the activation energy of this thin-film electrolyte is related to the deposition temperature [74].

Some sulfur-contained derivatives were also reported in addition to Si-doped LiPON derivatives. Joo *et al* first prepared the amorphous LiSON thin-film electrolyte by sputtering  $\text{Li}_2\text{SO}_4$  target on nitrogen atmosphere, whose highest ionic conductivity can reach  $2 \times 10^{-5} \text{ S cm}^{-1}$  on a certain sputtering condition and electrochemical window can be extremely wide (5.5 vs.  $\text{Li/Li}^+$ ) [75]. They also fabricated

LiBSO solid electrolyte, whose ionic conductivity can reach  $2.5 \times 10^{-6} \text{ S cm}^{-1}$  and the electrochemical window is about 5.8 V [76]. The structure of LiSON was confirmed by experimental and calculational method, which illustrated that the N atoms introduced in the sputtering process replace the O atoms and prevent the recrystallization of LiSON [77]. Kurzman *et al* synthesized  $\text{Li}_3\text{SO}_3\text{N}$  which contains rare  $[\text{SO}_3\text{N}]^{3-}$  polyanion by Brønsted acid-base reactions, but the ionic conductivity of this compound is very poor [78]. Mascaraque *et al* synthesized a kind of glass electrolyte LiPOSN by a melting process or mechanical milling, which shows a higher ionic conductivity than phosphate and oxynitride phosphate glass electrolytes with the same preparation method due to the introduction of S element [79, 80]. The 2D  $^{31}\text{P}$  NMR spectra of this LiPOSN electrolyte indicated that the phosphate groups containing S element are integrated into the formation of the phosphate network rather than clusters. Michel *et al* first prepared LiPSON solid electrolyte by RF-sputtering  $\text{Li}_2\text{SO}_4\text{--Li}_3\text{PO}_4$  mixed target, in which the ratio of double-coordinated nitrogen and triple-coordinated nitrogen ( $N_d/N_t$ ) shows a great impact on ionic conductivity of LiPSON electrolyte, and the highest ionic conductivity of LiPSON is about  $1.58 \times 10^{-5} \text{ S cm}^{-1}$ , that is comparable with the conductivity of LiSON electrolyte [81]. They also investigated the interface between LiPSON electrolyte and metallic Li, indicating that the production from the interfacial reaction is less beneficial for ionic conductivity [82]. The LiPSON thin-film electrolyte was used for all-solid-state electrochromic devices by Lupo *et al* [83].

Although LiPON manifests excellent electrochemical stability, ionic conductivity and mechanical strength in thin-film batteries, the change of oxidation state of P element during cycling can cause the variation in electronic conductivity [84]. Several research groups confirmed that the oxidation state of B is much more stable than that of P element [84]. Thus, Kim *et al* made a LiBON solid electrolyte as one of the LiPON analogs prepared by reacting sputtering under nitrogen plasma, which manifests the outstanding ionic conductivity of  $2.3 \times 10^{-6} \text{ S cm}^{-1}$  [84]. The FTIR and XPS analysis of LiBON illustrated that the N atoms substituted the O atoms in the  $x\text{Li}_2\text{O--B}_2\text{O}_3$  target and were incorporated into the Li-B-O matrix in the LiBON electrolyte. Additionally, the increase of  $\text{Li}_2\text{O}$  and the N-substitution in electrolyte caused the change of structure of borate from a ring-type one ( $\text{B}_2\text{O}_3$ ) to an open structure one ( $\text{B--O(N)--B}$ ), which creates more free space for higher mobility of  $\text{Li}^+$ . Dusszaue *et al* used FTIR analysis and DFT calculation to investigate the structural changes of LiBON after being prepared by the sputtering method as well as its mechanism of improving  $\text{Li}^+$  conductivity [85]. It was found out that the nitrogen tends to form only B–N–B bridge bonds between two triangular boron units, which is opposite to the structure of LiPON with  $N_t$  and  $N_d$  nitrogen bonds. The increase of ionic conductivity in borate glass after introducing N atoms may be due to the charge delocalization within the B–N–B bridges and the reduction of electrostatic interaction with  $\text{Li}^+$  ions. The LiBON thin-film electrolyte prepared by sputtering the  $\text{LiBO}_2$  target in the  $\text{N}_2$  atmosphere was also reported by Birke and Weppner [86].



LiPON electrolyte was likewise synthesized by the solid reaction from  $\text{LiNO}_3$ ,  $\text{Li}_2\text{CO}_3$ , and  $\text{B}_2\text{O}_3$  [87]. Song *et al* fabricated flexible thin-film batteries LCO/LiPON/Li on mica substrates with perfect mechanical properties on the bending condition, which showed outstanding capacity retention of 90% on the 1000th cycle [88]. Wu *et al* fabricated the LiBPON solid electrolyte by using the RF magnetron sputtering method in the  $\text{N}_2$  atmosphere with the Li-B-P-O system as the target [89]. The LiBPON electrolyte deposited on a high-temperature substrate demonstrated higher ionic conductivity than that on a substrate with room temperature. The ‘mixed former effect’ and incorporation of N created more Li vacancy and more cross-link structure for improving the mobility of  $\text{Li}^+$  ion. Yoon *et al* also prepared LiBPON electrolyte by sputtering  $\text{Li}_3\text{PO}_4$ - $\text{Li}_3\text{BO}_4$  mixed target, and most of the B atoms introduced in LiPON successfully replaced P sites [90]. Raman and XPS spectra indicated that the  $\text{N}_t$  was dominant in the LiBPON electrolyte, indicating the difference different from the LiPON, in which the amount of  $\text{N}_d$  atoms is more than  $\text{N}_t$  atoms, and the ASSTFBs based on the LiBPON thin-film electrolyte manifested excellent cycling performance and initial capacity.

Other nonmetallic elements doped into LiPON electrolytes were reported as well. LiPFON electrolyte was prepared by doping fluorine into LiPON through a new melting process, and the results illustrated that the substitution of O by N or F atoms increases the ionic conductivity due to the higher amount of Li in LiPFON through this synthesis route [91]. Lately, our research group also reported a new carbon-doped LiCPON solid electrolyte by RF magnetron sputtering method [92]. The LiCPON electrolyte showed higher ionic conductivity and air stability than the LiPON electrolyte. The data from XPS, XAS, and PDF analyses illustrated that C was successfully incorporated in the LiPON matrix film as the mixed glass former effect, and the C–N bridge bonding with the  $\text{CO}_3^{2-}$  ( $\text{CO}_2\text{N}^{3-}$ ) group is one of the major structural features. Furthermore, we also fabricated ASSTFBs of  $\text{LiFeFe}[\text{CN}]_6/\text{LiCPON}/\text{Li}$  with two unit cells externally connected in parallel and series, respectively.

In addition to introducing non-metallic elements into the LiPON electrolyte, LiPON derivatives doped with some metal atoms are introduced. Jee *et al* prepared a kind of tungsten-incorporated solid electrolyte of LiPWON by sputtering  $\text{Li}_3\text{PO}_4$  with  $\text{WO}_3$ , but it is not used in ASSTFBs due to the potential short circuiting [93]. Chen *et al* prepared LiAlTiPO solid electrolyte by sputtering  $\text{Li}_{1.3}\text{Al}_{0.3}\text{Ti}_{1.7}(\text{PO}_4)_3$  target, and the higher temperature of the substrate during deposition is conducive to the formation of the denser and smoother LiAlTiPO electrolyte film, which could induce higher ionic conductivity [94]. Tan *et al* firstly reported that the LiAlTiPON solid electrolyte was prepared by the sputtering method in the  $\text{N}_2$  atmosphere, and the thin-film electrolyte showed the highest ionic conductivity of  $1.22 \times 10^{-5} \text{ S cm}^{-1}$  when the substrate temperature was  $500^\circ\text{C}$  in the deposition process [95]. They thought that the substitution of N for O in electrolyte creates more crosslinking structure and decreases the electrostatic energy for  $\text{Li}^+$  migration. In addition, the mixed structural effect of partial polycrystalline and amorphous glassy electrolyte may be another reason for high ionic

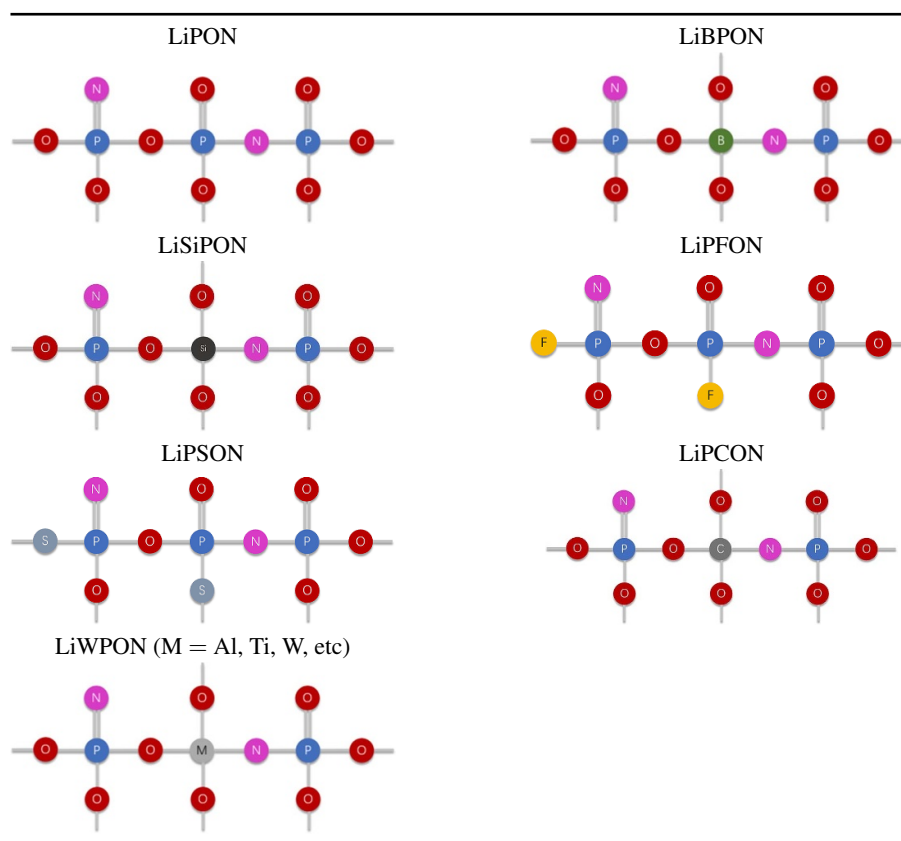
conductivity. Luo *et al* introduced a small amount of  $\text{La}_2\text{O}_3$  in LiAlPON solid electrolyte, in which the ionic conductivity of the electrolyte can be improved without obvious change in the network [96]. The N-doped LAGP thin-film electrolyte was prepared by magnetron sputtering method and an annealing process, whose ionic conductivity is  $2.3 \times 10^{-4} \text{ S cm}^{-1}$ . The addition of N element into LAGP makes the  $\text{PO}_4^{3-}$  tetrahedral units facilitate the facial  $\text{Li}^+$  diffusion [97].

Table 1 summarizes the structural diagram of these LiPON derivatives mentioned above, in which the incorporation of N, Si, B, S, C, F, and metal (M) elements into amorphous  $\text{Li}_3\text{PO}_4$  changes the distribution of the phosphate anion chains. According to the substitution position of doped elements for O in the structure of amorphous phosphate glass, these derivatives can be divided into two categories. Similar to the substitution of oxygen position by nitrogen, one is the substitution of sulfur or fluorine anion for O. The other is the mixed glass structure with C, Si, B, or M and P as the mixed glass former effect. These doped elements are incorporated into LiPON glass as nitrogen incorporation of the mixed glass with  $\text{CO}_3^{2-}$ ,  $\text{SiO}_4^{2-}$ ,  $\text{BO}_3^{2-}$  and  $\text{MO}_3^{2-}$  (or  $\text{MO}_4^{2-}$ ) structure in the cross-linked glass network of  $\text{Li}_3\text{PO}_4$ , respectively. Their chemical formula, ionic conductivity, and activation energy are listed in table 2. It is evident that most of these thin-film LiPON-based derivatives exhibit higher ion conductivities than those of LiPON. Undoubtedly, the investigation of these LiPON-based derivatives provides valuable information on the relationship between structure and properties. More works are still needed to develop LiPON-based derivatives for a suitable structure desirably and higher conductivity.

### 3. Interfaces of LiPON with electrodes

The interfaces of LiPON between anode and cathode play a critical role in the electrochemical performance of the batteries [98]. Therefore, it is necessary to investigate the interface property of LiPON before its large-scale application in energy storage devices. ASSTFB is an ideal research system to explore the electrolyte-electrode properties which have compactness, homogeneity, and smoothness for both electrode and electrolyte. This kind of battery system can simplify the research due to its clear structure and the distinctiveness of each component [99]. In all ASSTFBs, Li/LiPON/LCO is a classic one that has been commercialized. It consists of lithium cobalt oxide cathode, lithium metal anode, and LiPON solid electrolyte. This ASSTFB can be used as a research object to study the interface performance between the LiPON and the electrode. In addition to LCO cathode, the interface between other cathode materials and LiPON has been studied.

Interface impedance is one of the important interface properties between LiPON and the cathode. Iriyama *et al* explored the charge transfer reaction and charge transfer resistance of the LiPON/LCO interface in Li/LiPON/LCO batteries after thermal treatment [100]. The thermal treatment after the formation of the LiPON/LCO interface can improve the electrochemical reactivity of the ASSTFBs. According to the impedance spectra and Arrhenius equation, the activation energy of the charge transfer reaction remains unchanged before and

**Table 1.** The structural characteristic of LiPON-derivatives.

after heating treatment, but the charge transfer impedance decreases. Then the N1s XPS spectra of LiPON with and without thermal treatment show the ratio of  $N_t/N_d$  increased after thermal treatment. It implies that the crosslinking structure of the N atom in LiPON has changed after thermal treatment. The atomic rearrangement in this structural change increases the number of electrochemical active centers at the LiPON/LCO interface, resulting in the improvement of battery reactivity. Jeong *et al* studied the modified interface between LiPON and LCO [98]. One thin layer of aluminum oxide ( $Al_2O_3$ ) as the interface layer was prepared by using RF magnetron sputtering technique. The composition characterization structure of the LiPON/ $Al_2O_3$ /LCO interface by Auger electron spectroscopy reveals that the thickness of aluminum at the interface after heat treatment is greater than that in the as-deposited alumina, indicating that aluminum atoms are mixed with LCO to form a kind of solid solution  $LiCo_{1-y}Al_yO_2$ , which has very good ionic conductivity. Therefore, the introduction of the  $Al_2O_3$  layer and heat treatment can optimize the interface of LiPON/LCO for the improvement of the electrochemical performance battery. The effect of LiPON coating on the surface of LCO on the electrochemical performance and thermal stability of LCO cathode has been studied, which proves thermally stable LCO/LiPON [101].

The LiPON/LCO interfacial property in ASSTFB of Li/LiPON/LCO after a long cycle under high temperature was investigated by Wang *et al* [99]. An additional interface layer between LiPON and LCO was observed by the cross-sectional

TEM image of the battery (figure 9(a)), whose structure and composition are different from bulk LCO. It is a highly disordered structure and is composed of lithium oxide and cobaltous oxide by electron energy loss spectroscopy (EELS) analysis. After thermal treatment, a thicker disordered interface layer was observed in the cross-sectional TEM image of the LCO/LiPON interface (figures 9(b) and (c)), implying that the main mechanism of battery failure is the thermal effect rather than electrochemical activation. Jacke *et al* investigated the growth mechanism of LiPON on LCO cathode and their interface reaction by *in situ* XPS [102]. They found that some new nitrogen-containing species of  $NO_2^-$  and  $NO_3^-$  were formed before the formation of stoichiometric LiPON during the deposition process of LiPON on the surface of LCO at different temperatures. The ratio of  $N_t/N_d$  at the LiPON/LCO interface is higher than that in bulk, which indicates that the interface between LiPON and LCO is not an ion-conductive layer.

It is known that the redistribution of carriers will happen on the interface when two kinds of materials contact each other due to the difference in their chemical potential. It can form a space charge layer and establish an electric field which can cause band bending on the interface and the change of conductivity [103]. The work completed by Schwöbel *et al* revealed the energy level alignment on the interface of LiPON/LCO, which is obtained by *in situ* XPS measurement (figure 10(a)) [104]. The binding energy of each element was got according to the XPS spectra during the deposition



**Table 2.** The chemical formula, ionic conductivity, and activation energy of LiPON-derivatives.

Preparation method	Chemical formula	Ionic conductivity ( $\text{S cm}^{-1}$ at room temperature)	Activation energy (eV)	Reference
<b>Si-doped LiPON-derivatives</b>				
Rf magnetron sputtering	$\text{Li}_{2.3}\text{Si}_{0.2}\text{PO}_{1.4}\text{N}_{1.1}$	$5.65 \times 10^{-6}$	0.500	[66]
	$\text{Li}_{1.9}\text{Si}_{0.28}\text{PO}_{1.1}\text{N}_{1.0}$	$8.86 \times 10^{-6}$	0.491	[66]
	$\text{Li}_{2.9}\text{Si}_{0.35}\text{PO}_{1.5}\text{N}_{1.26}$	$1.00 \times 10^{-5}$	0.487	[66]
	$\text{Li}_{2.9}\text{Si}_{0.45}\text{PO}_{1.6}\text{N}_{1.3}$	$1.24 \times 10^{-5}$	0.479	[66]
Rf magnetron sputtering	$\text{Li}_{3.9}\text{Si}_{0.08}\text{PO}_{1.69}\text{N}_{1.52}$	$5.4 \times 10^{-6}$	0.47	[68]
	$\text{Li}_{4.2}\text{Si}_{0.39}\text{PO}_{2.75}\text{N}_{1.76}$	$6.6 \times 10^{-6}$	0.45	[68]
	$\text{Li}_{6.2}\text{Si}_{0.93}\text{PO}_{3.22}\text{N}_{2.14}$	$9.7 \times 10^{-6}$	0.41	[68]
Rf magnetron sputtering	$\text{Li}_{0.94}\text{Si}_{0.30}\text{P}_{0.70}\text{O}_{2.17}$	$1.49 \times 10^{-6}$	0.57	[69]
	$\text{Li}_{0.97}\text{Si}_{0.59}\text{P}_{0.41}\text{O}_{2.19}$	$2.00 \times 10^{-7}$	0.56	[69]
	$\text{Li}_{2.40}\text{Si}_{0.88}\text{P}_{0.12}\text{O}_{2.28}$	$4.09 \times 10^{-7}$	0.51	[69]
	$\text{Li}_{0.54}\text{Si}_{0.26}\text{P}_{0.74}\text{O}_{1.38}\text{N}_{0.76}$	$1.31 \times 10^{-8}$	0.58	[69]
	$\text{Li}_{0.56}\text{Si}_{0.56}\text{P}_{0.44}\text{O}_{1.22}\text{N}_{0.72}$	$2.81 \times 10^{-8}$	0.58	[69]
	$\text{Li}_{1.35}\text{Si}_{0.79}\text{P}_{0.21}\text{O}_{1.98}\text{N}_{0.98}$	$2.06 \times 10^{-5}$	0.45	[69]
	$\text{Li}_{0.89}\text{Ti}_2\text{Si}_{0.32}\text{P}_{3.8}\text{O}_{10.9}\text{N}_{2.52}$	$9.2 \times 10^{-6}$	0.29	[74]
<b>S-doped LiPON-derivatives</b>				
Rf magnetron sputtering	$\text{Li}_{0.29}\text{S}_{0.18}\text{O}_{0.53}$	$2.6 \times 10^{-6}$	N/A	[75]
	$\text{Li}_{0.29}\text{S}_{0.11}\text{O}_{0.60}$	$5.3 \times 10^{-6}$	N/A	[75]
	$\text{Li}_{0.29}\text{S}_{0.28}\text{O}_{0.38}\text{N}_{0.05}$	$1 \times 10^{-5}$	N/A	[75]
	$\text{Li}_{0.29}\text{S}_{0.28}\text{O}_{0.35}\text{N}_{0.09}$	$2 \times 10^{-5}$	N/A	[75]
Rf magnetron sputtering	LiBSO	$2.5 \times 10^{-6}$	0.51	[76]
Solid-state reaction	$\text{Li}_3\text{SO}_3\text{N}$	$\sim 10^{-14}$	1.03	[78]
Melting reaction	$\text{Li}_{1.62}\text{PO}_{2.84}\text{S}_{0.11}\text{N}_{0.32}$	$2.95 \times 10^{-7}$	0.64	[79]
Solid-state reaction	LiSPON	$1.4 \times 10^{-8}$ – $6.8 \times 10^{-7}$	N/A	[80]
Rf magnetron sputtering	LiSPON	$1.58 \times 10^{-5}$	N/A	[81]
Rf magnetron sputtering	LiSPON	$3.23$ – $9.75 \times 10^{-6}$	0.23–0.53	[83]
<b>B-doped LiPON-derivatives</b>				
Rf magnetron sputtering	$\text{Li}_{0.9}\text{BO}_{0.66}\text{N}_{0.98}$	$4.3 \times 10^{-9}$	N/A	[84]
	$\text{Li}_{3.09}\text{BO}_{2.53}\text{N}_{0.52}$	$2.3 \times 10^{-6}$	N/A	[84]
	$\text{Li}_{3.51}\text{BO}_{3.03}\text{N}_{0.52}$	$2.6 \times 10^{-7}$	N/A	[84]
Rf magnetron sputtering	LiBPON	$3.5 \times 10^{-6}$	0.53	[89]
Rf magnetron sputtering	$\text{Li}_{2.65}\text{B}_{0.11}\text{P}_{0.89}\text{O}_{3.00}\text{N}_{0.15}$	$6.88 \times 10^{-7}$	0.653	[90]
<b>Other kinds of LiPON-derivatives doped with the nonmetallic element</b>				
Melting reaction	LiPFO	$1.26 \times 10^{-7}$ – $6.61 \times 10^{-8}$	0.69–0.71	[91]
	LiPFON	$1.95 \times 10^{-7}$ – $5.74 \times 10^{-8}$	0.66–0.68	[91]
Rf magnetron sputtering	$\text{Li}_{3.25}\text{C}_{0.03}\text{PO}_{3.87}\text{N}_{0.21}$	$3.06 \times 10^{-6}$	0.43	[92]
<b>Metallic element (M) doped LiPON-derivatives</b>				
Rf magnetron sputtering	$\text{Li}_{3.426}\text{PW}_{0.008}\text{O}_{2.091}\text{N}_{0.364}$	$1.5 \times 10^{-7}$	0.51	[93]
Rf magnetron sputtering	Li-Al-Ti-P-O	$0.34$ – $2.46 \times 10^{-5}$	0.32–0.33	[94]
Rf magnetron sputtering	Li-Al-Ti-P-O-N	$1.22 \times 10^{-6}$ – $1.22 \times 10^{-5}$	0.44–0.63	[95]
Melting reaction	Li-La-Al-P-O-N	$1.47 \times 10^{-5}$	0.54	[96]
Rf magnetron sputtering	Li-Al-Ge-P-O-N	$2.3 \times 10^{-4}$	0.374	[97]

process (figure 10(b)). The core level of LCO shifts 0.3 eV to higher binding energy with time, implying that the LCO/LiPON has a downward band bending of 0.3 eV. According to the binding energy of the valence band maximum (VBM) of LCO and LiPON and their core level before and after LiPON deposition, the difference in their VBM can be calculated and the value of  $\Delta E_{\text{VBM}}$  is 1.26 eV. The change of work function  $\Delta\Phi$  is 0.25 eV and has a good agreement of the band bending, which indicates that the no large interface dipole is at the LCO/LiPON interface.

The formation and evolution of the LCO/LiPON interface before and during annealing were investigated by Fingerle *et al*

by way of XPS technique [105]. With the increase in annealing temperature, the interfacial reaction products ( $\text{LiNO}_2$ ,  $\text{Li}_2\text{O}$ , etc) between LCO and LiPON disappear. According to the species change at the interface during the annealing process, the chemical potential of elements can be derived with other additional data. The chemical potential of O element in LCO is higher than that in LiPON, as well as the Li element (figure 11(a)). The chemical potential of N element has maximum value around the LCO/LiPON interface because the N in  $\text{LiNO}_2$  is bound to LiPON after annealing. The band bending in the LCO cathode is attributed to the formation of electrostatic potential gradient and the band bending

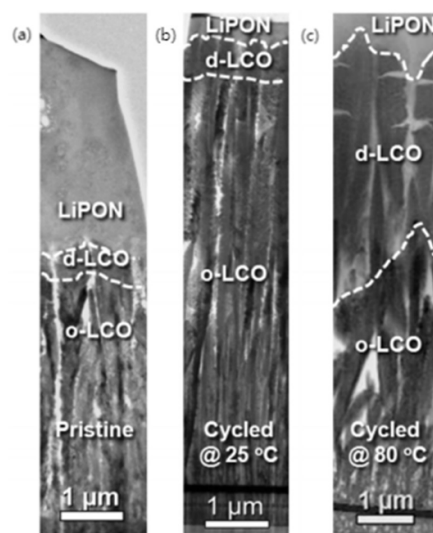


**Figure 9.** The cross-sectional TEM images of the (a) pristine LCO/LiPON interface, (b) the one was cycled at 25 °C, and (c) the one was cycled at 80 °C. Reprinted from [99]. Copyright (2016), with permission from Elsevier.

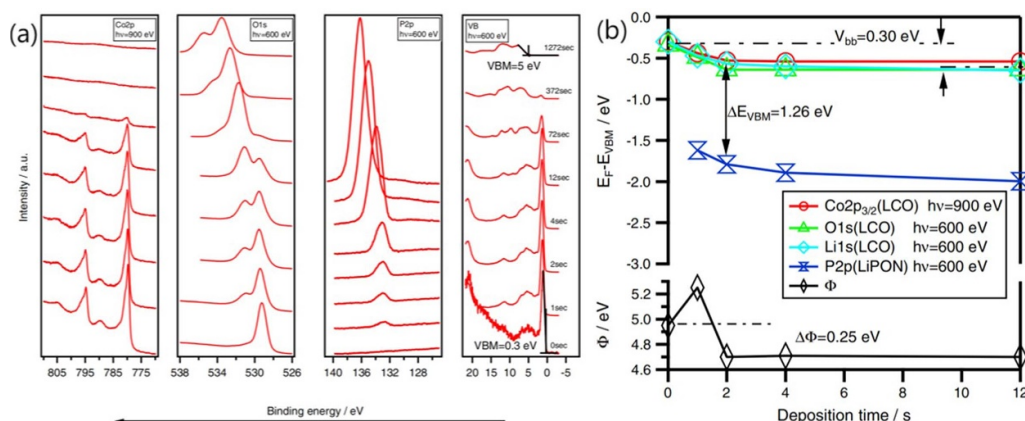


**Figure 10.** (a) XPS spectra of Co 2p, O 1s, P 2p, and the valence band at the LCO/LiPON interface with increasing LiPON coverage; (b) Change of the core levels of the LCO and the P 2p level of the LiPON layer with time. Reprinted from [104]. Copyright (2016), with permission from Elsevier.

has no change after annealing (figure 11(b)). The difference in electrochemical potential of Li-ion between LiPON and LCO causes the Li-ion to divorce from LCO and insert into LiPON, which results in the formation of Li-vacancies in LCO and Li-interstitials in LiPON. Both of them accumulate at the interface in their own phase, forming the space charge layer. The space charge layer influences the formation of other element defects, such as the O-vacancies. The defect formation energy is essential to understand the ionic properties and ionic structure, which can be identified by the difference of chemical potential to the relative energy level. The energy level gap reveals the difference in defect formation energy. The Li-ion energy level diagram can be drawn by calculating the defect formation energies and the diagram illustrates the presence of the space charge layer at the interface.

The interface between LiPON and other kinds of cathode materials was investigated. LiPON was coated on the surface of cathode material as an artificial interface layer to modify its

surface. Lv *et al* investigated the cycling performance and rate capability of high-voltage LNMO cathode with and without LiPON coating layer [106]. The LiPON coated LNMO shows better capacity and rate capability and less interfacial resistance than the pristine LNMO electrode. It was found that the ratio of content of  $\text{Mn}^{4+}/\text{Mn}^{3+}$  in LiPON coated LNMO is higher than that in pristine LiPON, indicating the formation of space charge layer between LiPON and LNMO and the oxygen vacancy moving from LiPON to LNMO. Yada *et al* studied the modification by dielectric material  $\text{BaTiO}_3$  (BTO) of the interface between LiPON and 5 V-class cathode  $\text{LiCr}_{0.05}\text{Ni}_{0.45}\text{Mn}_{1.5}\text{O}_{4-x}$  (LNM) [107]. Previous studies have shown that Li/LiPON/LNM cannot be charged and discharged at 3.0–5.3 V, which is attributed to the huge charge transfer resistance at the LiPON/LNM interface. It may be related to a huge electric potential difference between two materials. BTO nanoparticles can change the interfacial electric potential distribution and induce the Li-ion distribution at the interface,

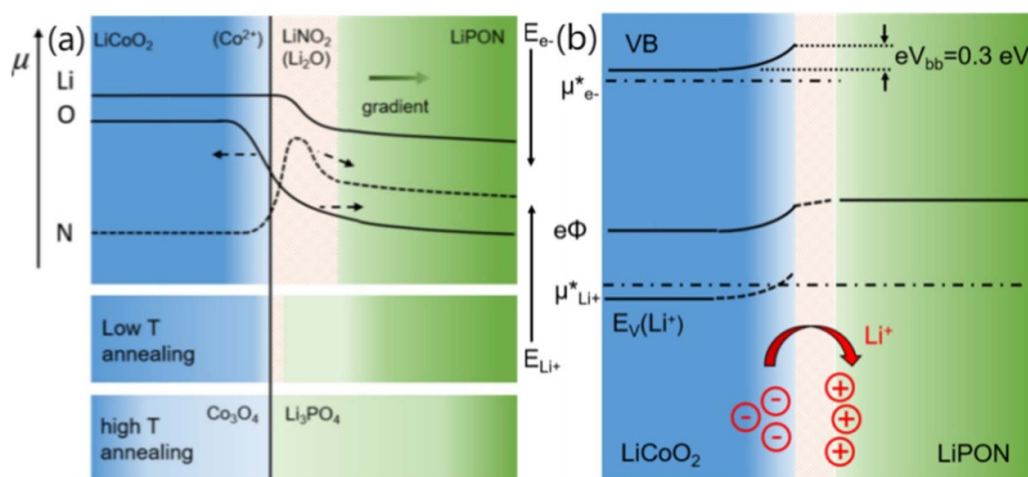


**Figure 11.** (a) Structure and composition of LCO/LiPON interface and its evolution during annealing. (b) Valence band bending, inner electric potential profile and Li-ion electrochemical potential at LCO/LiPON interface. Reprinted with permission from [105]. Copyright (2017) American Chemical Society.

which leads to the formation of the ‘Li-ion pathway’ for charge transfer reaction and reduction of interfacial resistance by four orders of magnitude.

The interface characteristics between LiPON and cathode were found related to the preparation method and experimental conditions. West *et al* delved into the electrical properties of thin-film LiPON prepared by the PLD method (LiPON-PLD) from a crystalline  $\text{Li}_2\text{PO}_2\text{N}$  target and by RF magnetron sputtering [108]. The LiPON-PLD layer displays lower charge transfer resistance with a higher amount of triply coordinated nitrogen and a relatively lower amount of doubly coordinated nitrogen. Cherkashinin *et al* made an investigation of the interfacial chemical composition and electronic properties when LiPON was deposited on the 5 V  $\text{LiCoPO}_4$  (LCP) and  $\text{LiNiPO}_4$  (LNP) cathodes [109]. The preparation method of cathode material has a great influence on the electronic properties of the interface between LiPON and cathodes, and a suitable preparation method is one of the possible ways to improve the interfacial stability.

Lithium metal is one of the most ideal anodes in solid-state batteries because of its extremely high theoretical capacity ( $3680 \text{ mAh g}^{-1}$ ) and low reduction electrode potential ( $-3.040 \text{ V vs. Standard Hydrogen Electrode}$ ) [110]. Therefore, it is of great significance to study the interfacial reaction and interfacial chemical composition between LiPON and metal lithium. Schwöbel *et al* investigated the interface formation and related reaction between LiPON and metal Li by *in situ* XPS [111]. After the evaporation of Li metal, some products on the surface of LiPON can be detected, such as  $\text{Li}_2\text{O}$ ,  $\text{Li}_3\text{N}$ ,  $\text{Li}_3\text{P}$ , and  $\text{Li}_3\text{PO}_4$ , indicating a chemical reaction between LiPON and Li metal to form new chemical species. The ratio of bridging oxygen and non-bridging oxygen ( $\text{O}_b/\text{O}_{nb}$ ) decreases after Li deposition, as well as the tendency of the ratio of  $\text{N}_i/\text{N}_d$ . This evidence indicates the LiPON network structure at the interface is destroyed after Li deposition due to the interface reaction between LiPON and Li metal.

However, they believe that the product of the interface reaction forms a passivation layer, which is thin enough to support the transfer of lithium ions. Hood *et al* utilized *in situ* electron microscopy to study the electrochemical stability and composition of the LiPON/Li interface [112]. They found that the interface reaction between Li metal and LiPON leads to the volume expansion of LiPON and the wetting of metal Li on the surface of LiPON. EELS elemental mapping shows two sublayers in the distribution of interface reaction products at the LiPON/Li interface. One is the O-rich and P-free interface layer directly connected with Li metal, and the other is the P-rich interface layer directly connected with LiPON. Among the binary products of  $\text{Li}_2\text{O}$ ,  $\text{Li}_3\text{N}$ , and  $\text{Li}_3\text{P}$ ,  $\text{Li}_3\text{P}$  is the only one with ionic and electronic conductivity. Its separation from Li metal inhibits the side reaction and improves the stability of the LiPON/Li interface. These binary products can theoretically enhance the electrochemical window and stabilize the interface. Xiao *et al* investigated the LiPON/Li interface properties in the ASSTFB, in which amorphous  $\text{V}_2\text{O}_{5-x}$  with many oxygen-vacancy sites was used as the cathode [113]. They utilized the facing target sputtering method which can prevent the film from plasma damage, to fabricate a uniform ultrathin  $\text{Al}_2\text{O}_3$  (UT-AO) film with low roughness between LiPON and Li anode. The interfacial evolution of LiPON/Li with and without UT-AO (1 nm) additional layer before and after two cycles was investigated by time-of-flight secondary ion mass spectrometry (TOF-SIMS). The TOF-SIMS depth profile shows the interfacial reaction between LiPON and Li, resulting in the consumption of Li metal and the formation of  $\text{Li}_2\text{O}$  and  $\text{Li}_3\text{P}$  by-products. However, there is no signal change at the interface with the presence of the UT-AO (1 nm) layer, which demonstrates the UT-AO layer suppresses the interface reaction and improves the stability of LiPON. The *ab initio* molecular dynamics (MD) simulations were used to study the interfacial interaction between LiPON and Li. The simulation results illustrate that the by-products from the



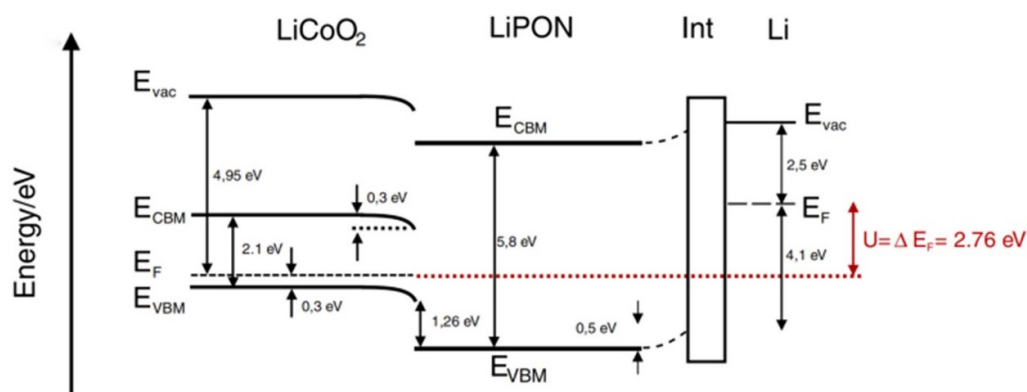


**Figure 12.** Complete energy band diagram of the LCO/LiPON/Li battery. Reprinted from [104]. Copyright (2016), with permission from Elsevier.

interfacial reaction, except  $\text{Li}_2\text{O}$ , have a strong chemical connection with Li metal, which is supported by the SEM spectra of the battery's cross-section. On the contrary to the interface without UT-AO, the lithiated  $\text{Al}_2\text{O}_3$  layer is thermodynamic and increases the stability of the Li/LiPON interface.

After using *in situ* XPS technique to investigate the properties of the LCO/LiPON interface, Schwöbel *et al* use the same method to reveal the energy alignment at the interface of Li/LiPON [104]. The initial XPS spectra of each element in LiPON illustrate that all the peaks shift about 1.5 eV to higher binding energy, which is related to the charge effect. The binding energy of Li 1s XPS at 53.4 eV is observed on the surface of metallic lithium, which is lower than the reference value (54.9 eV), indicating the presence of a space charge layer and band bending at the Li/LCO interface. The binding energy of VBM shifts 0.5 eV to lower binding energy, which illustrates band bending is 0.5 eV to upwards direction. The difference in the binding energy of VBM ( $\Delta E_{\text{VBM}}$ ) between Li metal and LiPON is calculated to be 4.1 eV. Combining the data of both the LCO/LiPON and Li/LiPON interface can draw a total energy band profile of ASSTFB of Li/LiPON/LCO (figure 12). The difference in Fermi level between LCO cathode and Li anode is the cell voltage, which is calculated to be 2.76 eV and is close to the experimental value (2.8 eV). Moreover, the electron chemical potential makes a major contribution to the cell voltage and only 11% of voltage attributes to the Li-ion chemical potential.

Sicolo *et al* conducted an investigation into the interfacial instability and side reactions at the interface of LiPON and Li by using surface science techniques and quantum computation methods [114]. The interface model of LiPON/Li was established by quantum simulation and the Li atom can diffuse from bulk metal Li to the LiPON without barriers, leading to the breaking of the network structure of LiPON and atomic rearrangement at the LiPON/Li interface. The thermal stability of the LiPON/Li interface is calculated and the results illustrate that the LiPON can be spontaneously reduced by Li metal in thermodynamics and the products include  $\text{Li}_2\text{O}$ ,  $\text{Li}_3\text{N}$ ,  $\text{Li}_3\text{P}$ , and lithium phosphate. These byproducts form a passivation layer on the Li/LiPON interface and prevent from further reaction of LiPON with Li metal. UPS and XPS

spectra also prove the formation of these chemical species. You *et al* used *ab initio* MD simulations to study the local structure of the interface of amorphous-LiPON/Li(100) and crystalline- $\text{Li}_2\text{PO}_2\text{N}(100)/\text{Li}(100)$  and the diffusion property of Li-ion at the LiPON/Li interface [115]. The atom at the original LiPON/Li interface diffuse to each other to form a new interfacial layer. The calculation results indicate that the diffusion of Li-ion at the LiPON/Li interface is faster than that in the bulk LiPON, which is related to the structural change at the interface. According to the simulation results, there is about 20% of Li-ion forming the tetrahedral structure like  $\text{Li}[\text{O}_2\text{N}_2]$ ,  $\text{Li}[\text{O}_3\text{N}]$ , and  $\text{Li}[\text{O}_4]$  in bulk LiPON. In the tetrahedral structure, Li is located at the center of the structure thus the diffusion of Li-ion is difficult and the ionic conductivity of Li-ion is very low. However, at the interface layer, the amount of these kinds of tetrahedral structures are less than those in bulk LiPON, as well as the decrease in the average coordination number of Li–O, Li–N, P–O, and P–N bond. Li-ion is less affected by the ionic bond of O and N due to the change in interfacial structure and coordination number, which results in the diffusion of Li-ion being less hindered. The conductivity of Li-ion at the interfacial layer is higher (2–3 orders of magnitude) than that of the bulk LiPON, which indicates that the interfacial layer has some positive effect on the performance of batteries.

The interface properties of LiPON with electrodes are essential to the performance of batteries. In ASSTFB, LiPON is considered to be one of the best solid electrolytes to build better interfaces with representative LCO and metal lithium, respectively. Many spectroscopic characterization methods such as *in situ* SEM, TEM, XRD, and EELS were used for studying the composition and structure of the interface layer due to their reaction between LiPON with electrodes. Besides, some special equipment is also utilized for investigation, such as DAISY-BAT (Darmstadt's Integrated System for battery Research) [102, 105, 111, 114]. Some strategies were taken to improve the properties of the interface layer, such as thermal treatment and the addition of other layers between LiPON and electrode. The gap in the energy level between LiPON and electrode derives from the difference in electrochemical potential of Li-ion in different materials. The equilibrium of

the electrochemical potential of Li-ion leads to the rearrangement of ions at the interface, which causes the formation of a space charge layer at the interface and the establishment of the internal electric field. This kind of electric field changes the conductive properties at the LiPON-electrode interface. Therefore, besides interesting aspects of the complex interface chemistry of the LiPON/electrode system, it is a great challenge to realize a perfect interface engineering for high performance of thin-film batteries. It needs to optimize electrode materials and preparation methods, preparation conditions, ultra-thin interface layer construction, and post-treatment.

#### 4. Preparation methods for LiPON

The preparation and synthesis of LiPON are generally considered as the insertion of N atoms or replacing O atoms with N atoms into the amorphous or polycrystalline structure of  $\text{Li}_3\text{PO}_4$ . However, the chemical activity of  $\text{N}_2$  is not enough to insert into the structure composed of the P–O bond. N plasma is induced by physical preparation methods such as magnetron sputtering, PLD technology, or nitrogen plasma-assisted deposition of electron beam evaporation as shown in figure 13, in which the plasma emission plume in the deposition process of LiPON thin films is produced by these methods. The bridging  $\text{N}_\text{d}$  and non-bridging apical  $\text{N}_\text{a}$  connect to P atoms are proposed for the possible pathway for the nitridation of  $\text{Li}_3\text{PO}_4$ . The electrochemical and physical properties of LiPON are reported to be strongly dependent on their preparation methods. They are briefly introduced as follows.

RF magnetron sputtering is the most commonly used preparation technique. In a typical magnetron sputtering equipment,  $\text{Li}_3\text{PO}_4$  is used as the target, and  $\text{N}_2$  is used as the reactive gas [116]. A mixed target of  $\text{Li}_3\text{PO}_4$  and  $\text{Li}_2\text{O}$  has also been attempted to increase the ionic conductivity of the deposition film [116]. In addition to pure nitrogen, mixtures with other gases such as argon and helium are also used [58]. Its deposition parameters such as substrate temperature, substrate-to-target distance, reactive gas pressure, sputtering power, and sputtering time determine the deposition rate as well as the properties of the LiPON film, including but not limited to the microstructure of the film and LiPON's electric properties [117]. For example, studies have shown that the islet microstructure may emerge accompanied by the elevated support temperature [117]. Compared with other preparation methods, the LiPON film obtained by RF magnetron sputtering has relatively higher ionic conductivity. However, the deposition rate of this method is relatively slow and the deposition area is usually limited. The former is determined by the mechanism of magnetron sputtering, and the latter is bound by the substrate-to-target distance and the size of the target [60]. As a physical deposition technique, it is difficult to obtain a highly-conformal step-coverage film onto the patterned surface with a high aspect ratio [118].

In contrast, PLD has a higher deposition rate. This technique contains a rotating holder to load the  $\text{Li}_3\text{PO}_4$  target. As for the substrate, it is mounted opposite the target, just a few centimeters apart. The most critical part is the ultraviolet

laser beam focused on the rotating target at a certain angle of incidence. According to the previous research, the fluence of the ultraviolet laser beam and  $\text{N}_2$  pressure can significantly affect the ionic conductivity of LiPON film. First, increasing the laser fluence can improve the quantity of N atoms incorporated into  $\text{Li}_3\text{PO}_4$  within limited, which is beneficial for higher ionic conductivity of LiPON electrolyte. However, the laser fluence has a certain threshold beyond which the ionic conductivity is probably saturated. Besides, higher  $\text{N}_2$  pressure within limited is favorable for increasing the ionic conductivity of LiPON, but excessive pressure can also be negative to the preparation of LiPON due to the contraction of the plume region. Similar to RF magnetron sputtering, substrate-to-target distance in the PLD technique is also influential to the surface roughness of LiPON electrolyte [58]. In addition to higher deposition rates, the PLD technique has other advantages, for example, the film can be deposited in ambient gases and the thickness of deposition film is relatively easy to control. However, the coagulated droplets would be present during the deposition process, which is unfavorable for the preparation of homogeneous LiPON electrolyte without roughness on the surface. At the same time, the deposition area of PLD is limited, and the nitridation efficiency is unsatisfactory.

To obtain better nitridation efficiency, ion beam assisted deposition (IBAD) is used to prepare LiPON thin film. In a typical IBAD system, in addition to the regular  $\text{Li}_3\text{PO}_4$  target and substrate, it additionally contains two ion sources, one of which provides a kind of ion beam to control the sputter atoms from the target, and the other one provides another ion beam to bombard the target. With the adjustment of the flow ratio of the reactive gas and the process gas, the nitrogen content of LiPON can be effectively adjusted [119]. Correspondingly, the hardness, elastic modulus, and the residual stress of LiPON film also change over the flow ratio. Research has shown that as the flow ratio of reactive gas and process gas increases within a certain range, the residual stress will decrease while the hardness will increase [119]. It is worth mentioning that in the IBAD system, the substrate is spatially separated from the sputter plasma, which is believed to help reduce the formation of an interfacial reactive layer [116]. The biggest disadvantage of IBAD is that the process is complicated and the deposition area is small. To obtain a larger deposition area, LiPON film can be also prepared using e-beam evaporation. The core component of the equipment employed in this technique is the e-beam evaporator, which is attached to an inductively coupled plasma reactor and other regular parts [60]. The larger deposition area, as well as the higher uniformity of the film, originate from the long substrate-to-target distance up to 40 cm. While having a faster deposition rate, this method is less efficient in nitriding. Likewise, same as RF magnetron sputtering and PLD, e-beam evaporation is limited to planar substrates because of shadow effects and film rupture may occur because of thermal tensile stress coming from the temperature difference between the substrate and the deposited film [120].

The target-based format dictates that all kinds of LiPON film obtained by the methods above are planar. However, in the application process, researchers prefer to conformally

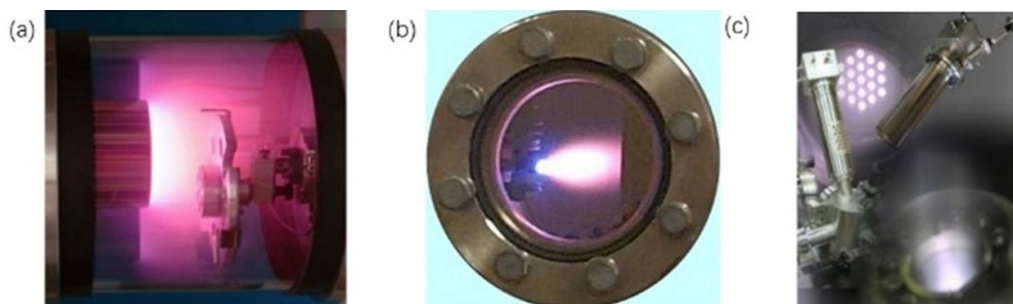


**Figure 13.** Plasma plume photos of (a) radio frequency magnetron sputtering; (b) pulsed laser deposition; (c) ion beam assisted deposition.

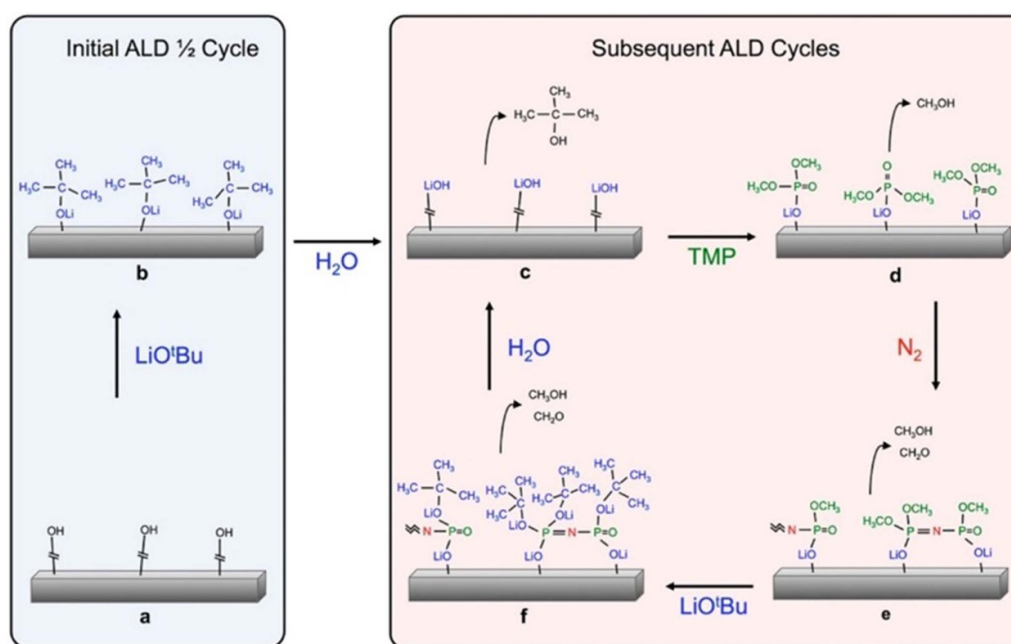


**Figure 14.** The flow chart of atomic layer deposition for LiPON. Reprinted with permission from [121]. Copyright (2015) American Chemical Society.

coat high aspect ratio nanostructures with thin, uniform layers, atomic layer deposition (ALD) and metal-organic CVD (MOCVD) can meet this requirement. On the one hand, these two methods can deposit a kind of homogeneous and highly-conformal film on highly structured substrates. On the other hand, they also get rid of the shackles of lithium phosphate and even nitrogen. That is to say, as long as there are precursors that can provide P element and N element, they may be used to prepare LiPON thin films.

In a typical quaternary ALD process (figure 14), four precursors including lithium tert-butoxide (LiO'Bu), deionized H<sub>2</sub>O, trimethylphosphate (TMP), and plasma N<sub>2</sub>, are used to deposit the LiPON film [121]. First, the argon carrier gas is used to transport LiO'Bu into the ALD chamber. Then H<sub>2</sub>O is introduced to participate in the reaction, thereby obtaining smaller LiOH units on the substrate. The third step is to add TMP to get surface-bound methyl phosphate species. However, the phosphate species obtained at this time are separated from each other, to cross-link them with each other, it is necessary to add the core precursor, i.e. plasma N<sub>2</sub> [121]. That is, in this step, the N content in the final LiPON film can be regulated

by changing the duration of the N pulse. Atomic-scale thickness controllable thin film deposition can be achieved by setting the number of cycles or reaction time. As for the precursors that do not participate in the reaction and reaction by-products, they can be blown out of the reaction chamber with the inert gas. Unfortunately, the deposition rate in the ALD method is relatively slow [120], and the ionic conductivity of the LiPON film is slightly lower than the film based on lithium phosphate and nitrogen. To improve the ionic conductivity, ALD processes using different precursors are being developed [122]. At the same time, in order to control deposition rates and film properties, ALD requires a specialized apparatus [71], which is not conducive to the popularization of this method.

In a classic MOCVD case (figure 15(a)), lithium dipivaloyl-methane (Li(DPM)), triethyl phosphate (TEP), and NH<sub>3</sub> are used as precursor materials to prepare LiPON thin film [123]. During the process flow, the vaporized Li(DPM) and TEP are brought into the reaction chamber by nitrogen [123]. Vapor deposition is achieved by regulating the flow rates of the three precursor gases. With the increasing temperature of the



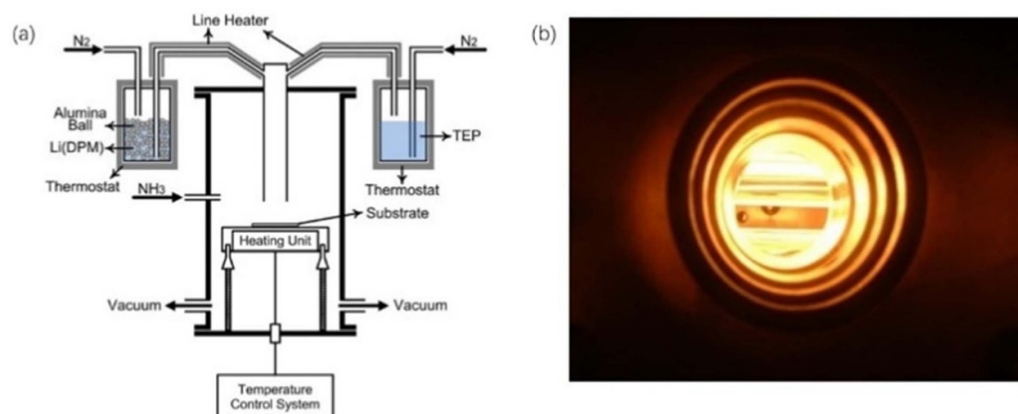


**Figure 15.** (a) Schematic illustration of metal-organic chemical vapor deposition equipment. Reprinted from [123]. Copyright (2013), with permission from Elsevier. (b) Schematic diagram of the effect of metal-organic chemical vapor deposition.

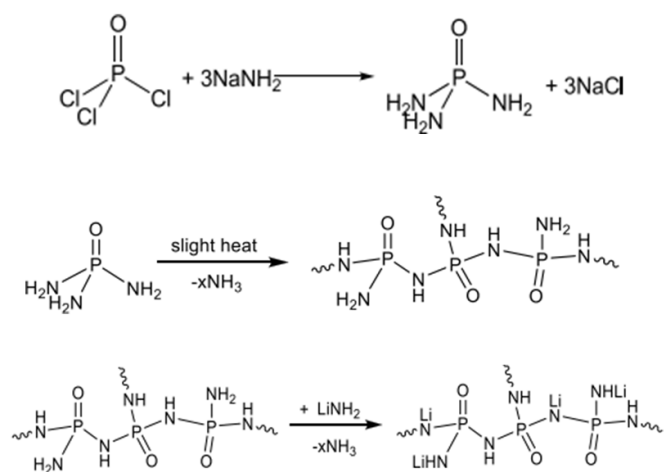
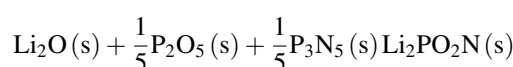


**Figure 16.** Reaction equation for preparing LiPON by polymer precursor method. Reprinted with permission from [71]. Copyright (2020) American Chemical Society.

substrate, while the deposition rate increases, the ratio of  $N_t$  to  $N_d$  also increases, which helps to improve the ionic conductivity of LiPON film. The main purpose of using metal organics as precursors is to maintain a low growth temperature, thereby effectively reducing the defect density in the film. The constituent elements of the film enter the reaction chamber in the form of gas, and the composition of the film can be controlled by the mass flow meter and the switch. At the same time, various properties of the epitaxial layer can be controlled by precisely controlling the flow of various gases. This method can obtain better thin-film samples on many amorphous substrates, which is mainly due to the lower reaction barrier, which reduces the orientation requirements of the substrate. Most importantly, MOCVD is an industrial-oriented method suitable for large-area thin film growth and mass production. Adducts are formed within a certain temperature range and it is a big problem because the deposition rate can be restricted by the presence of adducts, and the gas line may be blocked.

What makes matters worse is that carbon-containing polymeric by-products can severely reduce the conductivity of the prepared film [123].

All the methods described above require specific and complex instruments to complete gas phase deposition. In fact, satisfactory LiPON film can also be prepared by simple chemical reactions. For example, one of the simplest structures of the LiPON has been prepared by the following reaction equation through a high-temperature solid-state reaction method [124]:



In the product, the planar P-N-P-N backbone is stabilized by the N 2p  $\pi$  states, which contributes to its stability at high temperatures as well as in the ambient environment [124]. In another example, the polymer precursor method is also used to produce LiPON film (figure 16) [71]. First, phosphoramidate  $\text{OP}(\text{NH}_2)_3$  is obtained by ammonolysis of  $\text{OPCl}_3$ . Step-wise condensation reactions are then completed before the Li source is added for lithiation to obtain LiPON. This synthesis route permits the control of Li contents by varying the degree of lithiation, which is difficult to achieve using other methods, especially for gas-phase-based techniques. Meanwhile, the ratio of N content and P content is higher and the electrochemical stability window is wider. The above advantages enhance the ionic conductivity of the obtained LiPON film [71].

## 5. Conclusion and outlook

ASSTFBs have become one of the most efficient, reliable, clean, and sustainable energy storage devices. LiPON is one of the key components for perfecting the overall properties of ASSTFBs. In this review, we summarily introduced the recent development of ASSTFB based on LiPON and its applications. Due to the low conductivity of LiPON (far lower than that of liquid electrolyte), it is difficult to achieve high

energy densities of ASSTFBs, which limits its practical application. To improve the ionic conductivity and electrochemical stability of LiPON, the electrical properties and physical characteristics of various derivatives doped with B, C, F, Si, and other elements in amorphous structure are highlighted in this review. In addition, the morphology, composition, and electronic structure of the interface layer between LiPON and cathode materials as well as lithium metal anode are summarized, respectively. The thermodynamic stability and the decomposition kinetics of the LiPON/electrode interface layer were revealed. These investigations on the interface between LiPON/electrodes provide very important information for exploring high-quality interfaces. Further exploration of LiPON derivatives with higher ionic conductivity has the potential to improve their chemical stability and thus the electrochemical performance of ASSTFBs. Over the past ten years, advanced technologies were employed for the preparation of LiPON, such as ALD, CVD, and polymer precursor methods. Their own characteristics are described in this review. Among these methods, magnetron sputtering technology has been widely accepted as the most suitable preparation for LiPON thin film in fabricating these ASSTFBs. The low efficiency and high cost of these technologies is the main obstacle in these technologies for the large-scale preparation of LiPON thin film presently. Thin-film lithium batteries can generally be constructed into micron-sized thin-film batteries through a micromachining process to realize the so-called micro-battery. Thin-film batteries should be the best choice to realize energy miniaturization and integration such as three dimensions high-density integration of micro-batteries and an energy integrated system with micro-fuel cells, micro-photovoltaic cells, and micro-piezoelectric energy collectors for the self-generating and energy storage. The application of ASSTFBs within these devices is hopeful to revolutionize thin-film batteries.

## Acknowledgments

This work was financially supported by the NSAF (Grant No. U20A20336), and Tianmu Lake Institute of Advanced Energy Storage Technologies Scientist Studio Program [No. TIES-SS0002].

## ORCID iD

Zhengwen Fu  <https://orcid.org/0000-0002-4649-0194>

## References

- [1] Notten P H L, Roozeboom F, Niessen R A H and Baggetto L 2007 3D integrated all-solid-state rechargeable batteries *Adv. Mater.* **19** 4564–7
- [2] Jetybayeva A, Uzakbailu B, Mukanova A, Myung S-T and Bakenov Z 2021 Recent advancements in solid electrolytes integrated into all-solid-state 2D and 3D lithium-ion microbatteries *J. Mater. Chem. A* **9** 15140–78
- [3] Song J, Yang X, Zeng S-S, Cai M-Z, Zhang L-T, Dong Q-F, Zheng M-S, Wu S-T and Wu Q-H 2009 Solid-state microscale lithium batteries prepared with microfabrication processes *J. Micromech. Microeng.* **19** 045004
- [4] Kanehori K, Matsumoto K, Miyauchi K and Kudo T 1983 Thin film solid electrolyte and its application to secondary lithium cell *Solid State Ion.* **9–10** 1445–8
- [5] Lee H, Kim S, Kim K-B and Choi J-W 2018 Scalable fabrication of flexible thin-film batteries for smart lens applications *Nano Energy* **53** 225–31
- [6] Vallone M, Alleri M, Bono F and Catania P 2020 A new wireless device for real-time mechanical impact evaluation in a citrus packing line *Trans. ASABE* **63** 1–9
- [7] Lee H, Lim K Y, Kim K-B, Yu J-W, Choi W K and Choi J-W 2020 Hybrid thin-film encapsulation for all-solid-state thin-film batteries *ACS Appl. Mater. Interfaces* **12** 11504–10
- [8] Kutbee A T *et al* 2017 Flexible and biocompatible high-performance solid-state micro-battery for implantable orthodontic system *npj Flex. Electron.* **1** 7
- [9] Kanehori K, Ito Y, Kirino F, Miyauchi K and Kudo T 1986 Titanium disulfide films fabricated by plasma CVD *Solid State Ion.* **18–19** 818–22
- [10] Kirino F, Ito Y, Miyauchi K and Kudo T 1986 Electrochemical behavior of amorphous thin films of sputtered  $V_2O_5$ - $WO_3$  mixed conductors *Nippon Kagaku Kaishi* **1986** 445–50
- [11] Yamaki J 1996 Rechargeable lithium thin film cells with inorganic electrolytes *Solid State Ion.* **86–88** 1279–84
- [12] Ohtsuka H 1989 Electrical characteristics of  $Li_2O$ - $V_2O_5$ - $SiO_2$  thin films *Solid State Ion.* **35** 201–6
- [13] Ohtsuka H, Okada S and Yamaki J 1990 Solid state battery with  $Li_2O$ - $V_2O_5$ - $SiO_2$  solid electrolyte thin film *Solid State Ion.* **40–41** 964–6
- [14] Jones S D 1992 A thin film solid state microbattery *Solid State Ion.* **53** 628–34
- [15] Akridge J R and Vourlis H 1986 Solid state batteries using vitreous solid electrolytes *Solid State Ion.* **18–19** 1082–7
- [16] Akridge J R and Vourlis H 1988 Performance of  $Li/TiS_2$  solid state batteries using phosphorous chalcogenide network former glasses as solid electrolyte *Solid State Ion.* **28** 841–6
- [17] Jones S D, Akridge J R and Shokoohi F K 1994 Thin film rechargeable Li batteries *Solid State Ion.* **69** 357–68
- [18] Bates J B, Gruzalski G R, Dudney N J, Luck C F and Yu X H 1994 Rechargeable thin-film lithium batteries *Solid State Ion.* **70** 619–28
- [19] Bates J B 2000 Thin-film lithium and lithium-ion batteries *Solid State Ion.* **135** 33–45
- [20] Yu X H, Bates J B, Jellison G E and Hart F X 1997 A stable thin-film lithium electrolyte: lithium phosphorus oxynitride *J. Electrochem. Soc.* **144** 524–32
- [21] Neudecker B J, Dudney N J and Bates J B 2000 “Lithium-free” thin-film battery with *in situ* plated Li anode *J. Electrochem. Soc.* **147** 517–23
- [22] Whitacre J F, West W C and Ratnakumar B V 2003 A combinatorial study of  $Li_y Mn_x Ni_{2-x} O_4$  cathode materials using microfabricated solid-state electrochemical cells *J. Electrochem. Soc.* **150** A1676–83
- [23] West W C, Whitacre J F and Ratnakumar B V 2003 Radio frequency magnetron-sputtered  $LiCoPO_4$  Cathodes for 4.8 V thin-film batteries *J. Electrochem. Soc.* **150** A1660–66
- [24] Park Y-S, Lee S-H, Lee B-I and Joo S-K 1999 All-solid-state lithium thin-film rechargeable battery with lithium manganese oxide *Electrochem. Solid-State Lett.* **2** 58–59
- [25] Jeon E J, Shin Y W, Nam S C, Cho W I and Yoon Y S 2001 Characterization of all-solid-state thin-film batteries with  $V_2 O_5$  thin-film cathodes using *ex situ* and *in situ* processes *J. Electrochem. Soc.* **148** A318–22

- [26] Baba M 1999 Fabrication and electrochemical characteristics of all-solid-state lithium-ion batteries using  $V_2O_5$  thin films for both electrodes *Electrochem. Solid-State Lett.* **2** 320–2
- [27] Baba M, Kumagai N, Fujita N, Ohta K, Nishidate K, Komaba S, Groult H, Devilliers D and Kaplan B 2001 Fabrication and electrochemical characteristics of all-solid-state lithium-ion rechargeable batteries composed of  $LiMn_2O_4$  positive and  $V_2O_5$  negative electrodes *J. Power Sources* **97–98** 798–800
- [28] Baba M, Kumagai N, Fujita H, Ohta K, Nishidate K, Komaba S, Kaplan B, Groult H and Devilliers D 2003 Multi-layered Li-ion rechargeable batteries for a high-voltage and high-current solid-state power source *J. Power Sources* **119** 914–7
- [29] Creus R 1992 Thin films of ionic and mixed conductive glasses: their use in microdevices *Solid State Ion.* **53** 641–6
- [30] Menetrier M, Levasseur V, Delmas C, Audebert J F and Hagemuller P 1984 New secondary batteries for room temperature applications using a vitreous electrolyte *Solid State Ion.* **14** 257–61
- [31] Balkanski M, Julien C and Emery J Y 1989 Integrable lithium solid-state microbatteries *J. Power Sources* **26** 615–22
- [32] Creus R, Sarradin J, Astier R, Pradel A and Ribes M 1989 The use of ionic and mixed conductive glasses in microbatteries *Mater. Sci. Eng. B* **3** 109–12
- [33] Jourdain L 1988 Lithium solid state glass-based microgenerators *Solid State Ion.* **28** 1490–4
- [34] Kuwata N, Kawamura J, Toribami K, Hattori T and Sata N 2004 Thin-film lithium-ion battery with amorphous solid electrolyte fabricated by pulsed laser deposition *Electrochem. Commun.* **6** 417–21
- [35] Zheng S, Shi X, Das P, Wu Z-S and Bao X 2019 The road towards planar microbatteries and micro-supercapacitors: from 2D to 3D device geometries *Adv. Mater.* **31** 1900583
- [36] Koo M, Park K-I, Lee S H, Suh M, Jeon D Y, Choi J W, Kang K and Lee K J 2012 Bendable inorganic thin-film battery for fully flexible electronic systems *Nano Lett.* **12** 4810–6
- [37] Hallot M, Demortiere A, Roussel P and Lethien C 2018 Sputtered  $LiMn_{1.5}Ni_{0.5}O_4$  thin films for Li-ion micro-batteries with high energy and rate capabilities *Energy Storage Mater.* **15** 396–406
- [38] Trask J, Anapolsky A, Cardozo B, Januar E, Kumar K, Miller M, Brown R and Bhardwaj R 2017 Optimization of 10- $\mu$ m, sputtered,  $LiCoO_2$  cathodes to enable higher energy density solid state batteries *J. Power Sources* **350** 56–64
- [39] Yamamoto T, Iwasaki H, Suzuki Y, Sakakura M, Fujii Y, Motoyama M and Iriyama Y 2019 A Li-free inverted-stack all-solid-state thin film battery using crystalline cathode material *Electrochem. Commun.* **105** 106494
- [40] Xia Q Y *et al* 2021 Tunnel intergrowth  $Li_xMnO_2$  nanosheet arrays as 3D cathode for high-performance all-solid-state thin film lithium microbatteries *Adv. Mater.* **33** 2003524
- [41] Sun S, Xia Q Y, Liu J Z, Xu J, Zan F, Yue J L, Savilov S V, Lunin V V and Xia H 2019 Self-standing oxygen-deficient  $\alpha$ - $MoO_{3-x}$  nanoflake arrays as 3D cathode for advanced all-solid-state thin film lithium batteries *J. Materiomics* **5** 229–36
- [42] Chen X B, Sastre J, Rumpel M, Flegler A, Singhania A, Bonner J B, Hoffmann P and Romanyuk Y E 2021 Photonic methods for rapid crystallization of  $LiMn_2O_4$  cathodes for solid-state thin-film batteries *J. Power Sources* **495** 229424
- [43] Chen X B, Sastre J, Aribia A, Gilshtein E and Romanyuk Y E 2021 Flash lamp annealing enables thin-film solid-state batteries on aluminum foil *ACS Appl. Energy Mater.* **4** 5408–14
- [44] Wang C L, Dai X Y, Guan X, Jia W S, Bai Y and Li J Z 2020  $LiCoO_2$  thin film cathode sputtered onto 500 °C substrate *Electrochim. Acta* **354** 136668
- [45] Zhang Y M, Marschlok A C, Takeuchi K J, Kercher A K, Takeuchi E S and Dudney N J 2019 Understanding how structure and crystallinity affect performance in solid-state batteries using a glass ceramic  $LiV_3O_8$  cathode *Chem. Mater.* **31** 6135–44
- [46] Yim H, Yu S-H, Baek S H, Sung Y-E and Choi J-W 2020 Directly integrated all-solid-state flexible lithium batteries on polymer substrate *J. Power Sources* **455** 227978
- [47] Gockeln M, Glenneberg J, Busse M, Pokhrel S, Madler L and Kun R 2018 Flame aerosol deposited  $Li_4Ti_5O_{12}$  layers for flexible, thin film all-solid-state Li-ion batteries *Nano Energy* **49** 564–73
- [48] Nishio K, Horiba K, Nakamura N, Kitamura M, Kumigashira H, Shimizu R and Hitosugi T 2019 Bottom-current-collector-free thin-film batteries using  $LiNi_{0.8}Co_{0.2}O_2$  epitaxial thin films *J. Power Sources* **416** 56–61
- [49] Nishio K, Nakamura N, Horiba K, Kitamura M, Kumigashira H, Shimizu R and Hitosugi T 2020 Low resistance at  $LiNi_{1/3}Mn_{1/3}Co_{1/3}O_2$  and  $Li_3PO_4$  interfaces *Appl. Phys. Lett.* **116** 053901
- [50] Fu Z-W 1999 Pulsed laser deposited  $Ta_2O_5$  thin films as an electrochromic material *Electrochem. Solid-State Lett.* **2** 600–1
- [51] Ding F 1999 Electrochromic properties of ZnO thin films prepared by pulsed laser deposition *Electrochem. Solid-State Lett.* **2** 418–9
- [52] Fu Z-W, Chen L-Y and Qin Q-Z 1999 Electrical characterization of  $Ta_2O_5$  films deposited by laser reactive ablation of metallic Ta *Thin Solid Films* **340** 164–8
- [53] Ding F, Fu Z W, Zhou M F and Qin Q Z 1999 Tin-based composite oxide thin-film electrodes prepared by pulsed laser deposition *J. Electrochem. Soc.* **146** 3554–9
- [54] Chu Y-Q and Qin Q-Z 2002 Fabrication and characterization of silver- $V_2O_5$  composite thin films as lithium-ion insertion materials *Chem. Mater.* **14** 3152–7
- [55] Wang Y and Qin Q-Z 2002 A nanocrystalline NiO thin-film electrode prepared by pulsed laser ablation for Li-Ion batteries *J. Electrochem. Soc.* **149** A873–78
- [56] Wang Y, Fu Z-W, Yue X-L and Qin Q-Z 2004 Electrochemical reactivity mechanism of  $Ni_3N$  with lithium *J. Electrochem. Soc.* **151** E162–67
- [57] Fu Z-W, Li C-L, Liu W-Y, Ma J, Wang Y and Qin Q-Z 2005 Electrochemical reaction of lithium with cobalt fluoride thin film electrode *J. Electrochem. Soc.* **152** E50–55
- [58] Zhao S L, Fu Z W and Qin Q Z 2002 A solid-state electrolyte lithium phosphorus oxynitride film prepared by pulsed laser deposition *Thin Solid Films* **415** 108–13
- [59] Zhao S L and Qin Q Z 2003 Li V Si O thin film electrolyte for all-solid-state Li-ion battery *J. Power Sources* **122** 174–80
- [60] Liu W-Y, Fu Z-W, Li C-L and Qin Q-Z 2004 Lithium phosphorus oxynitride thin film fabricated by a nitrogen plasma-assisted deposition of e-beam reaction evaporation *Electrochem. Solid-State Lett.* **7** J36–J40
- [61] Li C-L and Fu Z-W 2007 All-solid-state rechargeable thin film lithium batteries with  $Li_xMn_2O_4$  and  $Li_xMn_2O_{4+0.5}ZrO_2$  cathodes *Electrochim. Acta* **52** 6155–64
- [62] Liu W-Y, Fu Z-W and Qin Z 2008 A “lithium-free” thin-film battery with an unexpected cathode layer *J. Electrochem. Soc.* **155** A8–A13
- [63] Shi D-R, Fu J, Shadike Z, Cao M-H, Wang W-W and Fu Z-W 2018 All-solid-state rechargeable lithium metal battery



- with a Prussian blue cathode prepared by a nonvacuum coating technology *ACS Omega* **3** 7648–54
- [64] Bates J B, Dudney N J, Gruzalski G R, Zuh R A, Choudhury A, Luck C F and Robertson J D 1993 Fabrication and characterization of amorphous lithium electrolyte thin films and rechargeable thin-film batteries *J. Power Sources* **43** 103–10
- [65] Lacivita V, Westover A S, Kercher A, Phillip N D, Yang G, Veith G, Ceder G and Dudney N J 2018 Resolving the amorphous structure of lithium phosphorus oxynitride (LiPON) *J. Am. Chem. Soc.* **140** 11029–38
- [66] Lee S-J, Bae J-H, Lee H-W, Baik H-K and Lee S-M 2003 Electrical conductivity in Li–Si–P–O–N oxynitride thin-films *J. Power Sources* **123** 61–64
- [67] Lee S-J, Baik H-K and Lee S-M 2003 An all-solid-state thin film battery using LISIPON electrolyte and Si–V negative electrode films *Electrochem. Commun.* **5** 32–35
- [68] Su Y R *et al* 2017 Electrochemical properties and optical transmission of high Li<sup>+</sup> conducting LiSiPON electrolyte films *Phys. Status Solidi b* **254** 1600088
- [69] Famprikis T, Galipaud J, Clemens O, Pecquenard B and Le Cras F 2019 Composition dependence of ionic conductivity in LiSiPO(N) thin-film electrolytes for solid-state batteries *ACS Appl. Energy Mater.* **2** 4782–91
- [70] Temeche E, Zhang X and Laine R M 2020 Solid electrolytes for Li–S batteries: solid solutions of poly(ethylene oxide) with Li<sub>x</sub>PON- and Li<sub>x</sub>SiPON-based polymers *ACS Appl. Mater. Interfaces* **12** 30353–64
- [71] Temeche E, Zhang X and Laine R M 2020 Polymer precursor derived Li<sub>x</sub>PON electrolytes: toward Li–S batteries *ACS Appl. Mater. Interfaces* **12** 20548–62
- [72] Zhang X, Temeche E and Laine R M 2020 Li<sub>x</sub> SiON ( $x = 2, 4, 6$ ): a novel solid electrolyte system derived from agricultural waste *Green Chem.* **22** 7491–505
- [73] Zhang X, Temeche E and Laine R M 2020 Design, synthesis, and characterization of polymer precursors to Li<sub>x</sub>PON and Li<sub>x</sub>SiPON glasses: materials that enable all-solid-state batteries (ASBs) *Macromolecules* **53** 2702–12
- [74] Wu F, Liu Y, Chen R, Chen S and Wang G 2009 Preparation and performance of novel Li–Ti–Si–P–O–N thin-film electrolyte for thin-film lithium batteries *J. Power Sources* **189** 467–70
- [75] Joo K-H, Sohn H-J, Vinatier P, Pecquenard B and Levasseur A 2004 Lithium ion conducting lithium sulfur oxynitride thin film *Electrochem. Solid-State Lett.* **7** A256–58
- [76] Joo K H 2003 Thin film lithium ion conducting LiBSO solid electrolyte *Solid State Ion.* **160** 51–59
- [77] Müller C R, Johansson P, Karlsson M, Maass P and Matic A 2008 Structure of glassy lithium sulfate films sputtered in nitrogen: insight from Raman spectroscopy and *ab initio* calculations *Phys. Rev. B* **77** 094116
- [78] Kurzman J A, Jouan G, Courty M, Rosa Palacin M, Armand M and Recham N 2013 Brønsted acid–base reactions with anhydrous sulfamates as a pathway to [SO<sub>3</sub>N]<sup>3–</sup>-containing compounds: preparation of Li<sub>3</sub>SO<sub>3</sub>N *Solid State Sci.* **25** 28–32
- [79] Mascaraque N, Takebe H, Tricot G, Fierro J L G, Durán A and Muñoz F 2014 Structure and electrical properties of a new thio-phosphorus oxynitride glass electrolyte *J. Non-Cryst. Solids* **405** 159–62
- [80] Mascaraque N, Fierro J L G, Muñoz F, Durán A, Ito Y, Hibi Y, Harada R, Kato A, Hayashi A and Tatsumisago M 2015 Thio-oxynitride phosphate glass electrolytes prepared by mechanical milling *J. Mater. Res.* **30** 2940–8
- [81] Michel F, Kuhl F, Becker M, Janek J and Polity A 2019 Electrochemical and optical properties of lithium ion conducting LiPSON solid electrolyte films *Phys. Status Solidi b* **256** 1900047
- [82] Michel F, Becker M, Janek J and Polity A 2020 Investigations of the solid electrolyte interphase using x-ray photoelectron spectroscopy *in situ* experiment on the lithium-based solid electrolyte LiPSON *Phys. Status Solidi b* **257** 1900336
- [83] Lupo C, Michel F, Kuhl F, Su Y R, Becker M, Polity A and Schlettwein D 2021 Investigation of sputter-deposited thin films of lithium phosphorous sulfuric oxynitride (LiPSON) as solid electrolyte for electrochromic devices *Phys. Status Solidi b* **258** 2100032
- [84] Kim J M, Park G B, Lee K C, Park H Y, Nam S C and Song S W 2009 Li–B–O–N electrolytes for all-solid-state thin film batteries *J. Power Sources* **189** 211–6
- [85] Dussauze M, Kamitsos E I, Johansson P, Matic A, Varsamis C P E, Cavagnat D, Vinatier P and Hamon Y 2013 Lithium ion conducting boron-oxynitride amorphous thin films: synthesis and molecular structure by infrared spectroscopy and density functional theory modeling *J. Phys. Chem. C* **117** 7202–13
- [86] Birke P and Weppner W 1997 Electrochemical analysis of thin film electrolytes and electrodes for application in rechargeable all solid state lithium microbatteries *Electrochim. Acta* **42** 3375–84
- [87] Li S, Yunchao X and Zhuangqi H 2018 Dislocation structure in a single crystal nickel base superalloy during high cycle fatigue at 870 °C *Rare Metal. Mater. Eng.* **47** 3835–8
- [88] Song S-W, Lee K-C and Park H-Y 2016 High-performance flexible all-solid-state microbatteries based on solid electrolyte of lithium boron oxynitride *J. Power Sources* **328** 311–7
- [89] Wu F, Zheng Y, Li L, Tan G, Chen R and Chen S 2013 Novel micronano thin film based on Li–B–P–O target incorporating nitrogen as electrolyte: how does local structure influence chemical and electrochemical performances? *J. Phys. Chem. C* **117** 19280–7
- [90] Yoon Y, Park C, Kim J and Shin D 2013 The mixed former effect in lithium borophosphate oxynitride thin film electrolytes for all-solid-state micro-batteries *Electrochim. Acta* **111** 144–51
- [91] Mascaraque N, Tricot G, Revel B, Durán A and Muñoz F 2014 Nitrogen and fluorine anionic substitution in lithium phosphate glasses *Solid State Ion.* **254** 40–47
- [92] Xia H-Y *et al* 2021 A new carbon-incorporated lithium phosphate solid electrolyte *J. Power Sources* **514** 230603
- [93] Jee S H, Lee M-J, Ahn H S, Kim D-J, Choi J W, Yoon S J, Nam S C, Kim S H and Yoon Y S 2010 Characteristics of a new type of solid-state electrolyte with a LiPON interlayer for Li-ion thin film batteries *Solid State Ion.* **181** 902–6
- [94] Chen H, Tao H, Zhao X and Wu Q 2011 Fabrication and ionic conductivity of amorphous Li–Al–Ti–P–O thin film *J. Non-Cryst. Solids* **357** 3267–71
- [95] Tan G, Wu F, Li L, Liu Y and Chen R 2012 Magnetron sputtering preparation of nitrogen-incorporated lithium–aluminum–titanium phosphate based thin film electrolytes for all-solid-state lithium ion batteries *J. Phys. Chem. C* **116** 3817–26
- [96] Luo Z, Lu A, Liu T, Song J and Han G 2016 La<sub>2</sub>O<sub>3</sub> substitution in Li–Al–P–O–N glasses for potential solid electrolytes applications *Solid State Ion.* **295** 104–10
- [97] Mousavi T, Slattery I, Jagger B, Liu J, Speller S and Grovenor C 2021 Development of sputtered nitrogen-doped Li<sub>1+x</sub>Al<sub>x</sub>Ge<sub>2-x</sub>(PO<sub>4</sub>)<sub>3</sub> thin films for solid state batteries *Solid State Ion.* **364** 115613
- [98] Jeong E, Hong C, Tak Y, Nam S C and Cho S 2006 Investigation of interfacial resistance between LiCoO<sub>2</sub> cathode and LiPON electrolyte in the thin film battery *J. Power Sources* **159** 223–6
- [99] Wang Z, Lee J Z, Xin H L, Han L, Grillon N, Guy-Bouyssou D, Bouyssou E, Proust M and Meng Y S

- 2016 Effects of cathode electrolyte interfacial (CEI) layer on long term cycling of all-solid-state thin-film batteries *J. Power Sources* **324** 342–8
- [100] Iriyama Y, Kako T, Yada C, Abe T and Ogumi Z 2005 Charge transfer reaction at the lithium phosphorus oxynitride glass electrolyte/lithium cobalt oxide thin film interface *Solid State Ion.* **176** 2371–6
- [101] Choi K-H, Jeon J-H, Park H-K and Lee S-M 2010 Electrochemical performance and thermal stability of LiCoO<sub>2</sub> cathodes surface-modified with a sputtered thin film of lithium phosphorus oxynitride *J. Power Sources* **195** 8317–21
- [102] Jacke S, Song J, Cherkashinin G, Dimesso L and Jaegermann W 2010 Investigation of the solid-state electrolyte/cathode LiPON/LiCoO<sub>2</sub> interface by photoelectron spectroscopy *Ionics* **16** 769–75
- [103] Zhou Y-F, Yang M-Z, She F-Q, Gong L, Zhang X-Q, Chen J, Song S-Q and Xie F-Y 2021 Application of x-ray photoelectron spectroscopy to study interfaces for solid-state lithium ion battery *Acta Phys. Sin.* **70** 178801
- [104] Schwöbel A, Jaegermann W and Hausbrand R 2016 Interfacial energy level alignment and energy level diagrams for all-solid Li-ion cells: impact of Li-ion transfer and double layer formation *Solid State Ion.* **288** 224–8
- [105] Fingerle M, Buchheit R, Sicolo S, Albe K and Hausbrand R 2017 Reaction and space charge layer formation at the LiCoO<sub>2</sub>—LiPON Interface: insights on defect formation and ion energy level alignment by a combined surface science—simulation approach *Chem. Mater.* **29** 7675–85
- [106] Lv S, Li M, Luo X, Cheng J and Li Z 2020 High-voltage LiNi<sub>0.5</sub>Mn<sub>1.5</sub>O<sub>4</sub> thin film cathodes stabilized by LiPON solid electrolyte coating to enhance cyclic stability and rate capability *J. Alloys Compd.* **815** 151636
- [107] Yada C, Ohmori A, Ide K, Yamasaki H, Kato T, Saito T, Sagane F and Iriyama Y 2014 Dielectric modification of 5V-Class cathodes for high-voltage all-solid-state lithium batteries *Adv. Energy Mater.* **4** 1301416
- [108] West W C, Hood Z D, Adhikari S P, Liang C, Lachgar A, Motoyama M and Iriyama Y 2016 Reduction of charge-transfer resistance at the solid electrolyte—electrode interface by pulsed laser deposition of films from a crystalline Li<sub>2</sub>PO<sub>2</sub>N source *J. Power Sources* **312** 116–22
- [109] Cherkashinin G, Yu Z, Eilhardt R, Alff L and Jaegermann W 2020 The effect of interfacial charge distribution on chemical compatibility and stability of the high voltage electrodes (LiCoPO<sub>4</sub>, LiNiPO<sub>4</sub>)/solid electrolyte (LiPON) interface *Adv. Mater. Interfaces* **7** 2000276
- [110] Zhang X-Q, Cheng X-B and Zhang Q 2018 Advances in interfaces between li metal anode and electrolyte *Adv. Mater. Interfaces* **5** 1701097
- [111] Schwöbel A, Hausbrand R and Jaegermann W 2015 Interface reactions between LiPON and lithium studied by *in-situ* x-ray photoemission *Solid State Ion.* **273** 51–54
- [112] Hood Z D, Chen X, Sacchi R L, Liu X, Veith G M, Mo Y, Niu J, Dudney N J and Chi M 2021 Elucidating interfacial stability between lithium metal anode and li phosphorus oxynitride via *in situ* electron microscopy *Nano Lett.* **21** 151–7
- [113] Xiao C-F, Kim J H, Cho S-H, Park Y C, Kim M J, Chung K-B, Yoon S-G, Jung J-W, Kim I-D and Kim H-S 2021 Ensemble design of electrode–electrolyte interfaces: toward high-performance thin-film all-solid-state li–metal batteries *ACS Nano* **15** 4561–75
- [114] Sicolo S, Fingerle M, Hausbrand R and Albe K 2017 Interfacial instability of amorphous LiPON against lithium: a combined Density Functional Theory and spectroscopic study *J. Power Sources* **354** 124–33
- [115] You Y-W, Cui J-W, Zhang X-F, Zheng F, Wu S-Q and Zhu Z-Z 2021 Properties of lithium phosphorus oxynitride (LiPON) solid electrolyte—Li anode interfaces *Acta Phys. Sin.* **70** 136801
- [116] Nowak S, Berkemeier F and Schmitz G 2015 Ultra-thin LiPON films—Fundamental properties and application in solid state thin film model batteries *J. Power Sources* **275** 144–50
- [117] Belous A G, V'yunov O I, Kovalenko L L, Bohnke O and Bohnke C 2014 Synthesis of thin-film electrodes based on LiPON and LiPON-LLTO-LiPON *Russ. J. Electrochem.* **50** 523–30
- [118] Fujibayashi T, Kubota Y, Iwabuchi K and Yoshii N 2017 Highly conformal and high-ionic conductivity thin-film electrolyte for 3D-structured micro batteries: characterization of LiPON film deposited by MOCVD method *AIP Adv.* **7** 085110
- [119] Li G, Li M, Dong L, Li X and Li D 2014 Low energy ion beam assisted deposition of controllable solid state electrolyte LiPON with increased mechanical properties and ionic conductivity *Int. J. Hydrog. Energy* **39** 17466–72
- [120] Xie J, Oudenhoven J F M, Harks P-P R M L, Li D and Notten P H L 2015 Chemical vapor deposition of lithium phosphate thin-films for 3D all-solid-state li-ion batteries *J. Electrochem. Soc.* **162** A249–54
- [121] Kozen A C *et al* 2015 Atomic layer deposition of the solid electrolyte LiPON *Chem. Mater.* **27** 5324–31
- [122] Nisula M, Shindo Y, Koga H and Karppinen M 2015 Atomic layer deposition of lithium phosphorus oxynitride *Chem. Mater.* **27** 6987–93
- [123] Kim H T, Mun T, Park C, Jin S W and Park H Y 2013 Characteristics of lithium phosphorous oxynitride thin films deposited by metal-organic chemical vapor deposition technique *J. Power Sources* **244** 641–5
- [124] Senevirathne K, Day C S, Gross M D, Lachgar A and Holzwarth N A W 2013 A new crystalline LiPON electrolyte: synthesis, properties, and electronic structure *Solid State Ion.* **233** 95–101